GeroScience (2022) 44:173–194
https://doi.org/10.1007/s11357-021-00408-z

ORIGINAL ARTICLE

Accumulation of C-terminal cleaved tau is distinctly associated with cognitive deficits, synaptic plasticity impairment, and neurodegeneration in aged mice

Anjanet Loon · Frank Zamudio · Awa Sanneh · Breanna Brown · Shayna Smeltzer · Milene L. Brownlow · Zainuddin Quadri · Melinda Peters · Edwin Weeber · Kevin Nash · Daniel C. Lee · Marcia N. Gordon · Dave Morgan · Maj-Linda B. Selenica

Received: 3 February 2021 / Accepted: 18 June 2021 / Published online: 19 August 2021

Abstract C-terminal cleaved tau at D421 (ΔD421-tau) accumulates in the brains of Alzheimer's disease (AD) patients. However, it is unclear how tau truncation, an understudied tau post-translational modification, contributes to AD pathology and progression. Utilizing an adeno-associated virus (AAV) gene delivery-based approach, we overexpressed full-length tau (FL-tau) and ΔD421-tau in 4- and 12-month-old mice for 4 months to study the neuropathological impact of accumulation in young adult (8-month) and middle-aged (16-month) mice. Overall, we show that independent of the tau species, age was an important factor facilitating tau phosphorylation, oligomer formation, and deposition into silver-positive tangles. However, mice overexpressing ΔD421-tau exhibited a distinct phosphorylation profile to those overexpressing FL-tau and increased tau oligomerization in the middle-age group. Importantly, overexpression of ΔD421-tau, but not FL-tau

Anjanet Loon and Frank Zamudio share first authorship / contributed equally to this work.

Supplementary Information The online version contains supplementary material available at https://doi.org/10.1007/s11357-021-00408-z.

A. Loon · F. Zamudio · A. Sanneh · B. Brown · S. Smeltzer · Z. Quadri · D. C. Lee · M.-L. B. Selenica
Department of Pharmaceutical Sciences, College of Pharmacy, University of South Florida, 12901 Bruce B. Downs Blvd, Tampa, FL 33612, USA
e-mail: anjanet@mail.usf.edu

F. Zamudio
e-mail: fzamudio@mail.usf.edu

A. Sanneh
e-mail: asanneh07@gmail.com

B. Brown
e-mail: breannabrown@mail.usf.edu

S. Smeltzer
e-mail: shaynasmeltzer@gmail.com

Z. Quadri
e-mail: Zainuddin.Quadri@uky.edu

D. C. Lee
e-mail: dan.lee@uky.edu

M. L. Brownlow · M. Peters · E. Weeber · K. Nash · M. N. Gordon · D. Morgan
Department of Molecular Pharmacological & Physiology, Morsani College of Medicine, University of South Florida, 12901 Bruce B. Downs Blvd, Tampa, FL 33612, USA
e-mail: milene_lara@yahoo.com

M. Peters
e-mail: petersmm@health.usf.edu

E. Weeber
e-mail: eweeber@health.usf.edu

K. Nash
e-mail: nash@usf.edu

M. N. Gordon
e-mail: mngordon@msu.edu

D. Morgan
e-mail: scientistdave@gmail.com

in middle-aged mice, resulted in pronounced cognitive impairments and hippocampal long-term potentiation deficits. While both FL-tau and ΔD421-tau induced neuronal loss in mice with age, ΔD421-tau led to significant neuronal loss in the CA3 area of the hippocampus and medial entorhinal cortex compared to FL-tau. Based on our data, we conclude that age increases the susceptibility to neuronal degeneration associated with ΔD421-tau accumulation. Our findings suggest that ΔD421-tau accumulation contributes to synaptic plasticity and cognitive deficits, thus representing a potential target for tau-associated pathologies.

Keywords Tauopathy · Age · Truncated tau · Full-length tau · LTP · Entorhinal cortex · Cognition · Neurodegeneration

Introduction

Aging is the most significant risk factor for the progression of Alzheimer's disease (AD). However, among the hallmark neuropathological factors, heightened tau phosphorylation levels are key indicators of disease progression and represent promising therapeutic targets for AD. In its normal state, tau is a structural protein involved in microtubule assembly and stabilization [21]. In AD and a set of diseases classified as tauopathies, tau forms pathological neurofibrillary tangle structures (NFTs) consisting of aggregated and hyperphosphorylated caspase-cleaved species [8, 10, 74]. Cleaved tau isoforms, particularly, have been implicated in the progressive loss of axonal connections, synaptic dysfunction, and neuronal death associated with AD [3, 4, 20, 39, 66]. Consequently, several cleaved forms of tau have been identified, including asparagine endopeptidase-cleaved tau at N255 and N368 as well as caspase 2-cleaved tau at D314, all of which promote neurodegeneration [30, 51, 76, 81, 82]. Another such tau species is a product of the truncation of tau at the aspartic acid at 421 position (ΔD421), shown to enhance tau aggregation by acting as nucleation seeds promoting filamentous self-assembly in vitro and in vivo [2, 10, 26, 30, 47]. Notably, pre-synaptic ΔD421-tau is present in abundance in cortical synaptosomal fractions derived from mice overexpressing P301L tau [54, 57], as well as in post-mortem AD brains when compared to healthy controls [65]. Additionally, ΔD421 tau truncation enhances its secretion independent of cell death, contributing to prion-like seeding and propagation of pathological tau [19, 20, 25, 37, 67]. This is further supported by several studies suggesting that tau is released by healthy cells and tau-overexpressing cells [17, 40, 55]. While there is emerging evidence highlighting the presence and unique properties of ΔD421-tau, its contribution to pathology with age remains poorly studied.

This study used an in vivo viral gene delivery approach to examine the impact of FL-tau and ΔD421-tau accumulation on synaptic plasticity, neurodegeneration, and cognitive function in young adult and middle-aged mouse cohorts. Our findings show that ΔD421-tau overexpression, but not FL-tau, impairs learning and memory along with long-term potentiation (LTP) in middle-aged mice. These effects were accompanied by significant differences in the phosphorylation, oligomerization, and argyrophilic tau profiles between ΔD421- and FL-tau, which were exacerbated in the older mice. Lastly, our data shows that ΔD421-tau differentially worsened degeneration of neuronal populations in the middle-aged hippocampus and medial entorhinal cortex. Overall, our results show that ΔD421-tau accumulation displays distinct neurotoxic effects compared to FL-tau, and mouse age heightened susceptibility of the brain to neuropathology.

Materials and methods

AAV-tau vector generation

Human wild-type (wt) FL-Tau (4R2N, 441 amino acids) was inserted into a pET 7C bacterial vector

Z. Quadri · D. C. Lee · M.-L. B. Selenica
Sanders-Brown Center On Aging (SBCoA), College of Medicine, University of Kentucky, Lexington, KY, USA

M. N. Gordon · D. Morgan
Translational Neuroscience, College of Human Medicine, Michigan State University, Grand Rapids, MI 49503, USA

M.-L. B. Selenica (✉)
Department of Molecular and Cellular Biochemistry, College of Medicine, University of Kentucky, 800 S. Limestone St, Lexington, KY 40536, USA
e-mail: Maj-Linda.Selenica@uky.edu

(courtesy of the late Dr. L. Binder, Michigan State University) and transferred into a pTR2-MCS viral vector. Truncation of C-terminal tau (1–421 amino acids) was generated by deleting the last 20 amino acids on the C-terminal segment of the full-length tau protein and as previously described [22]. We will refer to this tau form as delta D421-tau (ΔD421-tau). Both FL-tau and ΔD421-tau were cloned into the Age I and Xho I cloning sites of the recombinant adeno-associated virus (rAAV) vector pTR2-MCS under the control of the hybrid CMV chicken beta-actin promoter. A hemagglutinin (HA) tag was fused in both viral constructs for visualization purposes at the N-terminal, which does not disrupt C-terminal-mediated tau folding and aggregation [48]. rAAV serotype 9 was generated using pAAV9 and pXX6 in HEK293 cells [16, 35].

Mice

The C57BL/6 J mice were bred in the vivarium of Byrd Alzheimer Institute, USF Health, and were subsequently injected intracranially with AAV9 viral particles. The AAV9-FL-tau, AAV9-ΔD421-tau, and AAV9-empty capsid expressing C57BL/6 J mice after 4-month post-injection are referred to in this work as young-adult (8 months) and middle-aged (16 months) based on their life history stages (Fig. 1A) [23]. All groups were stratified for sex, an equal number of males and females were included. The rTg4510 mice were bred to 16 months old by crossing the parental human P301L tau mutation with tetracycline-controlled transactivator (tTa) phenotypes as previously described [60]. The tTa transgene was carried in the 129S6 background strain, and rTg4510 mice were F1 hybrids of FVBx129S6.

Stereotaxic intracranial AAV injection procedure

The injection procedure was performed using the convection-enhanced delivery method described previously [16, 62]. Briefly, mice were anesthetized with 1.5% isoflurane in 100% oxygen and secured into a stereotaxic apparatus. The coordinates of injection were as follows: hippocampus (HPC): anteroposterior, − 2.7 mm,lateral ± 2.7 mm, dorsoventral − 3.0 mm from bregma; cortex (CX): anteroposterior, + 2.2 mm; and lateral ± 1.7 mm, dorsoventral − 3.0 mm, from bregma. A microsyringe injector and controller (Stoelting, Wood Dale, IL) were used to inject 2 ml of virus (2×10^{12} viruses/ml) at a constant rate of 2.5 ml/min through a CED needle in each placement. The needle was kept in place for 1 min following injection and then was raised slowly. rAAV9-FL-tau, rAAV9-ΔD421-tau, and rAAV9-empty capsid control mice were injected bilaterally in the hippocampus and cortex of wt mice at two different ages: 4-month (n = 8–10 animals/group) and 12-month-old mice (n = 16–17 animals/group). Mice were allowed to recover for 4 months prior to tissue collection.

Behavioral testing

Behavioral analysis was carried out as previously described [5, 13, 63]. Mice were handled by the same experimenter to monitor body weight throughout the experiment and to habituate the mice with the experimenter.

Two-day radial arm water maze (RAWM)

In this task, mice learned to use extra-maze spatial cues to locate the escape platform [5]. On day one, mice were given 15 trials where every three trials were averaged into one block (5 blocks in total), alternating between a visible platform (above the water) and a hidden platform (below the water) between trials. The next day (day 2), mice underwent 15 additional trials (5 blocks), with all the trials using a hidden platform. The goal arm location for sequential mice was different to avoid odor cues. Incorrect arm entries or failure to select an arm for 15 s were counted as errors. Twenty-four hours were allowed for each mouse to rest between the last trial of day one and the first trial of day 2.

Radial arm water maze reversal

This test was completed on the third day of the radial arm water maze (RAWM) test and was performed under similar conditions. The goal arm was positioned 180º from the original location to test the ability of mice to extinguish a learned memory and create a novel one. All 15 trials were performed with a hidden platform. For both tests, average and total numbers of errors for each trial were calculated to assess learning and working memory.

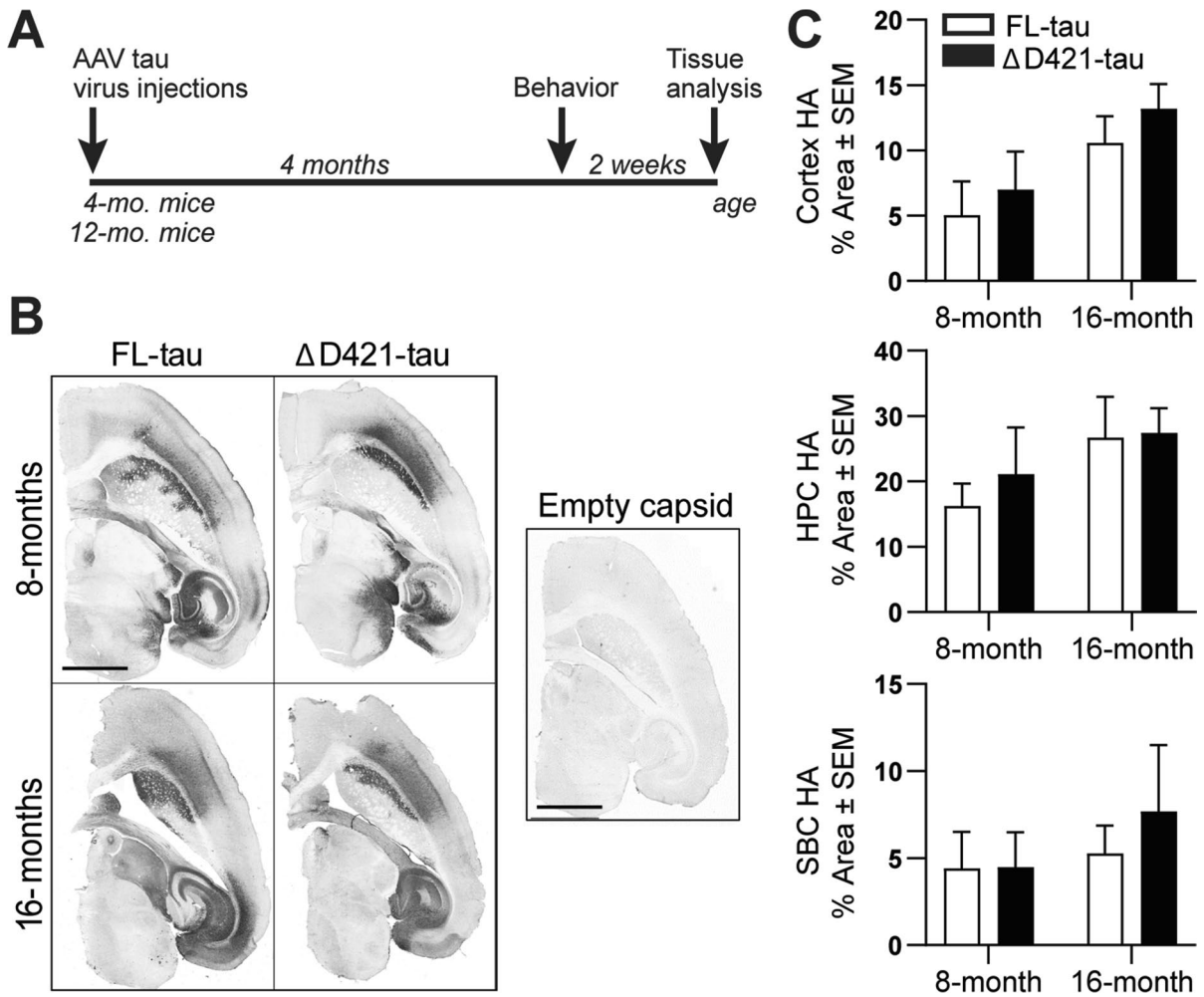

Fig. 1 Transgene expression in FL-tau and ΔD421-tau mice. **A** AAV viral in vivo tau gene transfer in 4- and 12-month-old wt mice for 4 months was followed by behavior testing. **B** Immunohistochemical staining of brain tissue for hemagglutinin (HA) expression. **C** Quantification of percent positive area in HA immunoreactivity in the cortex (CX), hippocampus (HPC), and subiculum (SBC) with age. Statistical analyses were performed by two-way ANOVA followed by Tukey post-hoc test (n = 7–8 animal/group). Scale bar represents 2000 μm

On the last day (24 h following reversal RAWM testing), all animals were tested in the open pool task with a visible platform in a different location to the acquisition and reversal to ensure that all mice could see and climb on the platform. Latency to find and ascend the platform was recorded (60 s maximum).

Open field

General anxiety and locomotor activity were measured by monitoring mice for 15 min in a walled open field box (Stoelting). The activity was recorded using ANY-maze video tracking software (Stoelting).

Rotarod

Motor function, coordination, and learning were measured by placing mice on an apparatus with a rotating rod (Rota-Rod Stoelting; AugoBasile Apparatus) that was accelerated at a steady rate to 40 rpm over 5 min. Latency to fall off from the rod was measured.

Y-maze

To assess working spatial memory, mice were placed in a walled Y-maze for a single 5-min trial.

The sequence of arm entries and the total number of arm choices were recorded. Spontaneous alternation, defined by entering all three arms of the maze sequentially without repetition, was calculated.

Novel object recognition

Short-term memory was evaluated in the novel object recognition test. Briefly, mice were placed in a 40 cm by 40 cm arena and monitored using ANY-maze video tracking software. Two similar objects were placed along the centerline of the arena, and each animal was given three 5-min trials for acclimation with a 5-min inter-trial interval. After each trial, the arena and object cues were cleaned to minimize olfactory cues. Five minutes after the acclimation trials, one of the objects was replaced with a novel object, and animals were given a 5-min trial during which object exploration was monitored.

Novel mouse recognition

Similar to the novel object recognition task, mice were subjected to a recognition test utilizing a different context consisting of three chambers separated by transparent plastic walls. After one 10-min habituation period, two mice were placed on the left and right chambers. In the second trial, the interaction between the test mouse with the other mice was measured using ANY-maze video tracking software. In the third trial, one of the mice was replaced with a novel mouse, and interaction was measured again. The chambers were thoroughly cleaned between trials to minimize olfactory cues.

Fear conditioning

To test long-term memory in associative learning, mice were placed in an enclosed fear conditioning apparatus for 3 min followed by a loud tone (70 dB of white noise) for 30 s paired with a 0.5-mA shock applied to the floor grid during the last 2 s of the conditioned stimulus. Another conditioned stimulus paired with a shock was given during the training trial after 2 min. For contextual memory, the mice were placed in the same fear conditioning apparatus and monitored for freezing for 3 min to the context 24 h after training without an auditory cue or shock. Immediately after the contextual test, mice were placed in a novel environment with different walls and floors along with an olfactory cue. Mice were allowed to explore the chamber for 3 min and then exposed to the conditioned stimulus (tone) for 3 min. Learning was assessed by measuring freezing behavior in the last 3 min.

Tissue collection

Four-month post-intracerebral injection, mice were weighed and overdosed with a euthanizing solution containing pentobarbital (Somnasol, Henry Schein). Cardiac perfusion was performed via gravity drip with 25 ml of 0.9% standard saline solution. Mice were placed on an isothermal pad after anesthesia and during perfusion to avoid artefactual tau phosphorylation caused by reductions in body temperature [53]. Brains were collected following saline perfusion and were hemisected down the sagittal midline. One hemisphere was dissected and frozen on dry ice for biochemical studies. The second hemisphere was immersion-fixed in 4% paraformaldehyde for 24 h and cryoprotected in successive incubations of 10%, 20%, and 30% solutions of sucrose for 24 h in each solution. Subsequently, the fixed hemispheres were frozen on a cold stage and sectioned in the horizontal plane (25-mm thickness) using a sliding microtome. Brain sections were stored in Dulbecco's phosphate-buffered saline (DPBS) with 10 mM sodium azide solution at 4 °C for immunohistochemical analysis of tau levels.

Electrophysiology recordings

Following behavioral testing, a cohort of 16-month-old ΔD421- and FL-tau-injected mice along with wt littermates (n=4/group) was euthanized, and the hippocampi were dissected for LTP recordings as previously described [70]. The brain was rapidly dissected and placed in ice-cold, oxygenated, cutting solution containing: 110 mM sucrose, 60 mM NaCl, 3 mM KCl, 28 mM $NaHCO_3$, 1.25 mM NaH_2PO_4, 5 mM glucose, 0.6 mM ascorbate, 7 mM $MgCl_2$, and 0.5 mM $CaCl_2$. Hippocampal slices (400 μm) were prepared on a vibratome and allowed to equilibrate in a 50% cutting saline and 50% artificial cerebrospinal fluid (ACSF) solution containing: 125 NaCl, 2.5 mM

KCl, 26 mM $NaHCO_3$, 1.25 mM NaH_2PO_4, 25 mM glucose, 1 mM $MgCl_2$, and 2 mM $CaCl_2$. Slices were maintained with a constant 95% O_2/5% CO_2 perfusion for 10 min before being transferred to the brain slice recording chamber supported by nylon mesh or maintained in a holding container. Slices were recovered for a minimum of 1 h before recording. The recording chamber was held at 30° ± 0.5 °C with an ACSF flow rate of 1 ml/min. Field excitatory postsynaptic potentials (fEPSPs) were recorded from the stratum radiatum in hippocampal area CA1 via glass microelectrodes filled with artificial cerebrospinal fluid (resistance 1–4 MΩ). Responses were generated by stimulation of Schaffer collaterals arising from the CA3 region. Stimulating electrodes consisting of formvar-coated nichrome wire delivered biphasic stimulus pulses (1–15 V, 100 µs duration, 0.05 Hz). Stimulation delivery was controlled by pClamp 9.0 software (Molecular Devices) via a Digidata 1322A interface (Molecular Devices) and a stimulus isolator (model 2200; A-M Systems). Signals were amplified using a differential amplifier (model 1800; A-M Systems), filtered at 1 kHz, and digitized at 10 kHz. For all experiments, baseline stimulus intensity was set at the level that elicited ~ 50% of the maximum fEPSP response as determined from the input–output curve. The input–output relationship was determined by stimulating slices from 0 to 15 mV at 0.5 mV increments. LTP was induced by a theta-burst stimulation (TB-stim) protocol, consisting of two trains of four pulse bursts at 100 Hz separated by 200 ms, repeated six times with an intertrain interval of 10 s. For analyses, the last 10 min of the recording was averaged and compared.

To measure the direct effects of ΔD421 tau, we incubated hippocampal slices from 16-month-old, tau naïve mice acutely with PBS, 150 µM FL-tau, or 150 µM ΔD421-tau protein (n = 4, recombinant protein was generously gifted by Dr. Kanaan, Michigan State University, MI). After 1-h bath perfusion, LTP was induced by two trains of tetanic stimulation, 100 Hz for 1 s and recorded using a test pulse frequency of 0.017 Hz and described [22].

Immunohistochemical/histological procedure and analysis

Eight sections, 200 mm apart, were chosen for histological analysis using immunohistochemical procedural methods described previously [62]. For each marker, floating sections from all animals were placed in multi-sample staining trays, and endogenous peroxidase was blocked (10% methanol, 3% H_20_2 in PBS, 15 min). Tissue samples were permeabilized (with 0.2% lysine, 1% Triton X-100 in PBS solution, 30 min) and incubated overnight in the appropriate primary antibody. Anti-N-terminus of human tau (H150, Santa Cruz, Dallas, TX, USA); anti-phospho-tau at Serine 396 (pS396, Anaspec, Freemont, CA, USA); anti-phospho-tau at Serine 202 and Threonine 205 (biotinylated AT8, ThermoScientific, Waltham, MA, USA); HA (biotinylated, Roche Diagnostic, Manheim, Germany) and NeuN (EMD Millipore, St. Charles, MO, USA) antibodies were used. Sections were rinsed 3 × in PBS and then incubated in corresponding biotinylated secondary antibody for 2 h, except AT8 and HA antibodies (Vector Laboratories, Burlingame, CA, USA). The tissue was again rinsed 3 × in PBS and incubated with Vectastain® Elite® ABC kit (Vector Laboratories, Burlingame, CA, USA) for enzyme conjugation. Finally, sections were developed using 0.05% diaminobenzidine, 0.5% Ni^{++}, and 0.03% H_2O_2. Tissue sections were then mounted onto slides, dehydrated, and coverslipped. Each immunochemical assay omitted few sections from primary antibody incubation to evaluate the nonspecific reaction of the secondary antibody.

Gallyas histology was performed using premounted sections and air-dried for a minimum of 24 h as previously described [63]. Sections were rehydrated for 30 s prior to proceeding with the Gallyas protocol. Slides were treated with 5% periodic acid for 5 min, washed with water, and incubated sequentially in silver iodide (1 min) and 0.5% acetic acid (10 min) solutions prior to being placed in developer solution (2.5% sodium carbonate, 0.1% ammonium nitrate, 0.1% silver nitrate, 1% tungstosilicic acid, 0.7% formaldehyde). To stop the reaction, 0.5% acetic acid solution was used, and slides were incubated in 0.1% gold chloride followed by 1% sodium thiosulfate, and counterstained with 0.1% nuclear fast red in 2.5% aqueous aluminum sulfate, each step separated by washes in water. Following a final wash, slides were dehydrated and coverslipped.

Stained sections were imaged using a Zeiss Mirax150 digital scanning microscope. The area of positive staining in each section was analyzed. The software used hue, saturation, and intensity (HSI) to

segment the image fields. Thresholds for object segmentation were established with images of high and low staining levels to identify positive staining and exclude background levels. During analysis, these limits were held constant across each given stain.

Neurodegeneration measurements by NeuN analysis

The hippocampus, subiculum, entorhinal cortex, and cortical regions were manually outlined using IAE analysis software (Zeiss, Germany). *The Mouse Brain in Stereotaxic Coordinates* was referenced for determining anatomical regions [52]. The hippocampus, subiculum, entorhinal cortex, and anterior cortex were manually outlined using IAE analysis software (Zeiss, Germany). The Mouse Brain in Stereotaxic Coordinates was referenced for determining anatomical regions [52]. The entorhinal cortex was divided into lateral and medial regions by examining spatial and concentration-based differences in cell body arrangement, according to the Allen Mouse Brain Atlas [6]. The staining density was measured in all regions and presented as a percent (%) of positive area. Thickness in layer II/III was measured using Mirax Viewer software (Zeiss Technologies, 10,594 Thornwood, USA). Values are presented as averages per animal within each treatment and age group. Error bars are presented as the standard error of the mean (SEM).

Biochemical analysis

Tissue samples were prepared for western analysis as previously described [15]. Briefly, the dissected anterior cortex and hippocampal tissue were weighed and resuspended in RIPA buffer (50 mM Tris, 140 mM NaCl, 10% NP40, 10% Na deoxycholate, 10% SDS, with protease inhibitor cocktail and phosphatase inhibitor cocktails I and II) (Sigma-Aldrich Corp., St. Louis, MO, USA) at ten volumes/weight of tissue. The tissue was homogenized with a motorized pestle followed by a brief (10 s) sonication pulse. Aliquots were collected at this point for biochemical analysis and referred to as "brain homogenate." Pierce BCA protein assay (Thermo Fisher Scientific, Waltham, MA, USA) was used to determine protein concentrations. For western analysis, 20 mg of protein was loaded for each sample. The antibodies against phosphorylated tau epitope pS262, pS199/202, and AT180 (Thr231) were obtained from Anaspec (Freemont, CA, USA), while the H150 antibody was obtained from Santa Cruz Biotechnologies (Dallas, TX, USA). Monoclonal PHF1 antibody was kindly provided by Dr. Peter Davies [14, 29, 34]. T22 antibody was kindly provided by Dr. Rakez Kayed [43]. The monoclonal HT7 antibody was purchased from Thermo Fisher Scientific (Waltham, MA, USA). For dot blots, proteins were applied onto a wet nitrocellulose membrane and dried by vacuum. Once dry, the membrane was blocked and developed with the T22 antibody as described above.

Reverse transcriptase-polymerase chain reaction (RT-PCR)

Total RNA from mouse hippocampi ($n = 3$) was extracted using Qiagen's All Prep DNA/RNA/Protein kit. Fifty nanograms of RNA were used to generate cDNA using Superscript II First Strand Synthesis System (Life Technologies). The cDNA was used on the real-time mouse synaptic plasticity RT^2 Profiler PCR Array (Qiagen, Catalog no. PAMM-126Z) using RT^2 SYBR ® Green qPCR Mastermix (Qiagen catalog no. 330529). Ct values were exported, and data was analyzed using the web portal provided by Qiagen (www.qiagen.com/geneglobe), which generated the top upregulated and downregulated genes. Volcano plots were generated using Qiagen Gene globe software (Qiagen, Germantown, MD, USA). Genes were classified into known pathways: immediate-early response genes (IEGs), neuronal receptors (NR), extracellular matrix molecules (ECM), long-term potentiation (LTP), postsynaptic density (PSD), cell adhesion molecules (CAM), long-term depression (LTD), and CREB cofactors (CREB).

Statistical analysis

Two-tailed Student's *t* test, one-way ANOVA, or two-way repeated-measures ANOVA with Fisher's least significance difference (LSD) or Tukey post-hoc tests were used as detailed in the figure legends. Values were considered significant if $p < 0.05$. Graphs were generated using GraphPad Prism 8.0 (La Jolla, CA, USA) analysis software.

Results

AAV9-injected mice exhibited no significant differences in viral expression

To investigate the pathological profiling of ΔD421-tau and FL-tau, we prepared adeno-associated virus serotype 9 (AAV9) particles containing HA-tags fused to the N-terminal of FL-tau and ΔD421-tau protein sequences. After 4-month post-injection, immunohistochemistry was performed to measure transgene expression in AAV9-FL-tau (4R2N), AAV9-ΔD421-tau, or AAV9-empty capsid-injected mice via quantification of HA immunoreactivity in the left hemisphere (Fig. 1A). We found similar viral expression across mice of both ages at the injection regions with no overt difference in spreading between FL-tau and ΔD421-tau, while empty capsid animals showed no visible HA staining (Fig. 1B). Quantitatively, viral transduction was readily detected at the injection regions, cortex (CX), and hippocampus (HPC), attaining a range of 5–15% and 20–30% of the measured areas (Fig. 1C). The transgene also resulted in expression in the subiculum, albeit with less immunoreactivity (SBC, 5–10%).

ΔD421-tau overexpression results in cognitive deficits in middle-aged mice

To assess whether FL- or ΔD421-tau overexpression affected the neurobehavioral phenotype, mice in both the young adult and middle-aged cohorts were tested for spatial navigation memory using the radial arm water maze task (RAWM) [5]. All mice swam well and showed no signs of distress nor signs of motor or visual impairments (data not shown). Young adult FL-tau and ΔD421-tau mice demonstrated normal learning and memory ability in the acquisition and reversal tasks (measured as the average of errors) since both groups achieved the criterion associated with optimal learning (< 2 errors per block) both in acquisition and reversal RAWM testing, similar to the empty capsid control group (Fig. 2A–D). However, we found that middle-aged mice performed significantly more total errors, but not average number of errors, than young adult mice in the control group, FL-tau and ΔD421-tau (Fig. 2A vs. B, D). Conversely, in the reversal phase, the middle-aged ΔD421-tau group performed more errors on average in each block when compared to control and FL-tau groups (Fig. 2C), resulting in a significantly greater number of total reversal errors (Fig. 2D). Interestingly, the number of average errors during reversal learning was significantly increased in the middle-aged ΔD421-tau group in block 1, but remained similar to those from the middle-aged FL-tau group by the final block 5 (Fig. 2C). Overall, middle-aged ΔD421-tau mice showed impaired learning in the reversal compared to age-matched controls, while middle-aged FL-tau animals performed significantly more errors on average, but not total errors than the middle-aged controls in the last block (Fig. 2B vs. Figure 2D). Thus, ΔD421-tau overexpression appears to consistently slow spatial learning in middle-aged mice under reversal conditions. The positive correlation between middle-aged ΔD421-tau levels and total RAWM errors is illustrated further by linear regression analysis (Fig. s1).

Given the spatial learning deficits observed in the ΔD421-tau middle-aged cohort, we decided to explore a more extensive battery of cognitive measures at this age. Therefore, another subset of middle-aged mice injected with AAV9-tau species or empty capsid control underwent open field, rotarod, Y-maze, novel object recognition, and context and cued fear conditioning testing. We found no changes in general anxiety, measured by the time mice spent in the center of an open field, and locomotor activity in middle-aged mice expressing either FL- or ΔD421-tau (Fig. s2A, B). While neither short-term spatial working memory in the Y-maze (Fig. s2C) nor short-term recognition memory in the novel object and mouse tests was affected by FL-tau or ΔD421-tau overexpression (Fig. s2D, E), we found that ΔD421-tau mice displayed significant impairment in motor learning during day 2 of the rotarod compared to the age-matched control group (Fig. 3A). Additionally, while fear memory acquisition (measured by the freeze time after receiving foot shocks paired with a tone) was similar between all groups (Fig. 3B), we found that ΔD421-tau mice displayed impaired long-term memory retrieval during context (Fig. 3C) or cue (Fig. 3D), suggesting a deficit in associative learning in this cohort.

ΔD421-tau accumulation impairs hippocampal long-term potentiation (LTP) induction in the middle-aged mouse brain.

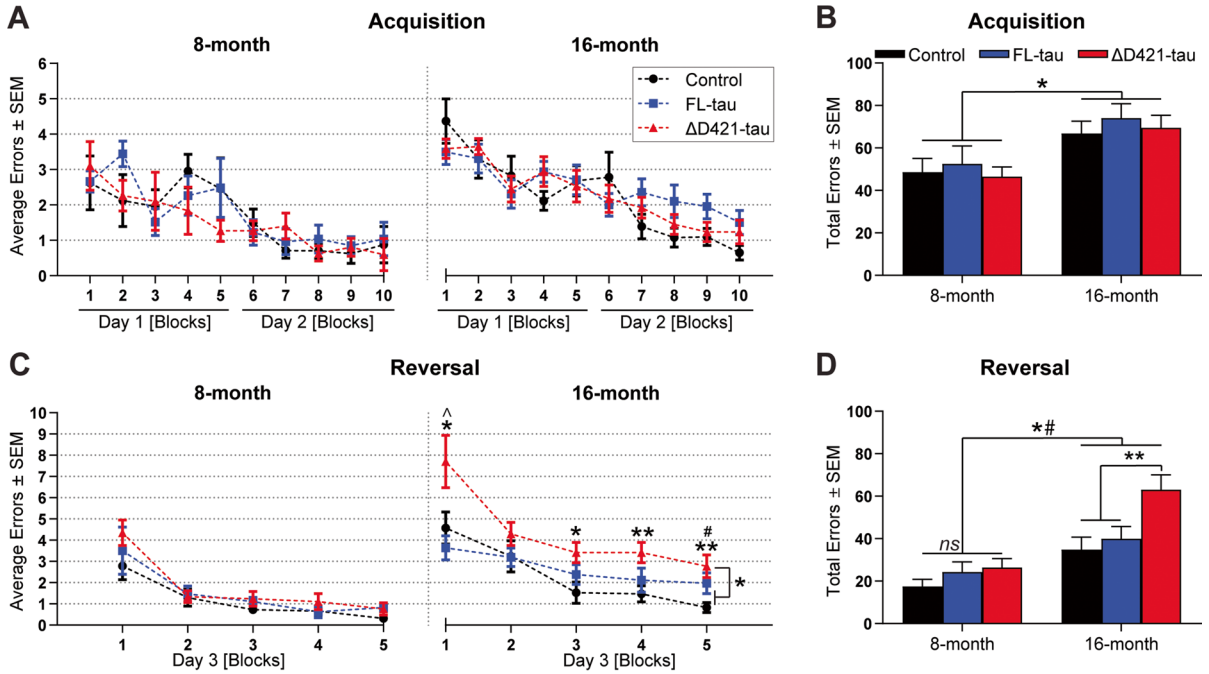

Fig. 2 ΔD421-tau, but not FL-tau, overexpression in the middle-aged mouse brain results in impairment of spatial memory performance. **A** The average number of errors per block for the radial arm water maze (RAWM) in young adult and middle-aged cohorts. **B** The total number of errors performed in the RAWM in the young adult and middle-aged cohorts. Statistics were performed by two-way ANOVA followed by Fisher's least significant difference (LSD) post-hoc test (n = 8–10 for the 8-month-old and n = 15–17 for the 16-month-old group, *p < 0.05). **C** The average number of errors per block for the RAWM reversal in young adult and middle-aged cohorts. Statistical analyses were carried out by two-way ANOVA followed by Fisher's least significance different (LSD) post-hoc test (n = 8–10 for young adult and n = 15–17 for middle-aged group, *p < 0.05 and **p < 0.01 between aged control and ΔD421-tau, ^p < 0.05 between aged FL-tau and ΔD421-tau, #p < 0.05 between aged control and FL-tau). **D** The total number of errors across all trials in the RAWM reversal in the young adult and middle-aged cohorts. Statistics were performed by two-way ANOVA followed by Fisher's least significant difference (LSD) post-hoc test (n = 8–10 for the young adult and n = 15–17 for the middle-aged group, *p < 0.05 between all 8-month-old treatment groups and 16-month-old control and FL-tau, **p < 0.01, #p < 0.001 between all 8-month-old treatment groups and 16-month-old ΔD421-tau)

Considering the hippocampal-dependent learning and memory deficits present in the middle-aged ΔD421-tau mice, we performed electrophysiology analysis of LTP in a subset of the middle-aged mouse cohort. Field excitatory postsynaptic potentials (fEPSPs) were recorded from the stratum radiatum in CA1 pyramidal neurons (Fig. 4A). We included hippocampal slices from the rTg4510 mouse model since LTP impairment in this mouse model of tauopathy was reported by several groups [1, 61, 79]. The tetanic stimulation of the Schaffer collaterals resulted in robust LTP in slices from the middle-aged control and FL-tau-expressing mice. However, the hippocampi from ΔD421-tau mice showed impaired LTP maintenance for 60 min after induction compared to control and FL-tau mice, as shown in the last 10-min analysis (Fig. 4B). As expected, hippocampal slices from rTg4510 mice demonstrated a significant impairment of LTP compared to control and FL-tau mice. Interestingly, hippocampal LTP recordings from the rTg4510 mice were not statistically different from the ΔD421-tau-expressing mice, suggesting a crucial effect of this tau species on LTP.

To further determine whether ΔD421-tau was directly responsible for the LTP deficits in middle-aged mice, we treated ex vivo hippocampal slices acutely with PBS, 150 µM FL-tau, or 150 µM ΔD421-tau recombinant protein and measured LTP as described previously [22](Fig. 4C). Recombinant ΔD421-tau treatment, but not FL-tau, robustly

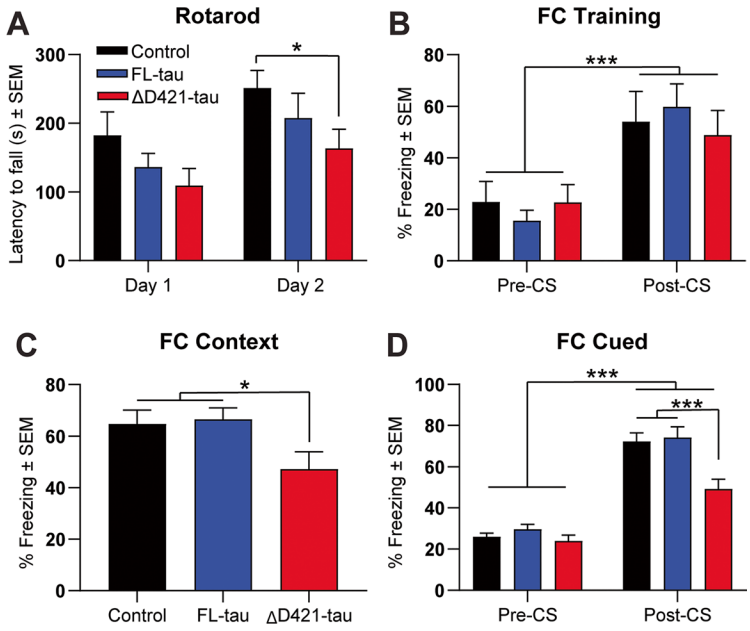

Fig. 3 ΔD421-tau, but not FL-tau, overexpression in the middle-aged mouse brain results in deficits in the rotarod and fear conditioning. **A** Latency to fall in the rotarod in days 1 and 2. Statistical analysis was performed by two-way ANOVA followed by Fisher's least significant difference (LSD) post-hoc test (n = 7–9, *p < 0.05). **B** Percent freezing measured in fear conditioning (FC) training before (pre-CS) and after (post-CS) a conditioned stimulus (tone) paired with foot shocks. Statistical analysis was performed by two-way ANOVA followed by Fisher's least significant difference (LSD) post-hoc test (n = 7–9, ***p < 0.001). **C** Percent freezing measured 24 h after fear conditioning (FC) training in the same context without an auditory cue. Statistical analysis was performed by one-way ANOVA followed by Fisher's least significant difference (LSD) post-hoc test (n = 7–9, *p < 0.05). (D) Percent freezing measured twenty-four hours after fear conditioning (FC) training in a different context before (pre-CS) and after (post-CS) a conditioned stimulus (cued tone). Statistical analysis was performed by two-way ANOVA followed by Fisher's least significant difference (LSD) post-hoc test (n = 7–9, ***p < 0.001)

impaired LTP compared to middle-aged control slices as measured in the last 10 min of analysis (Fig. 4D), suggesting ΔD421-tau can directly impair LTP. These results correlated well with alteration in the expression of several early and late induction genes involved in LTP (volcano plot, Fig. s3). Indeed, RT-qPCR analysis of RNA from middle-aged control and ΔD421-tau mouse hippocampi demonstrated down-regulation of early induction genes including *Mmp9*, *Adcy8,* and *Bdnf* (Tab s1), while upregulating others (Tab s2).

ΔD421-tau-overexpressing mice exhibit a distinct phosphorylation profile from FL-tau mice

Because the induced tau phosphorylation is an indicator of neuropathology, we performed immunohistochemical analyses to measure the tau phosphorylation profile achieved by each overexpressed tau protein. We focused on the hippocampus and the synaptically connected subiculum, a region known to be particularly vulnerable to D421 truncation in AD [27]. First, we measured the total tau levels (H150 immunoreactivity) expressed by each viral construct in both ages (Fig. 5A, B, boxes represent the magnified areas). Quantification revealed similar tau levels in the FL- and ΔD421-tau mice in the HPC (15–20%) and SBC (10–15%) in both young adult and middle-aged mice. Analysis of the CX showed similar tau expression (5–10%) (Fig. s4A, B). Similarly, the biochemical analysis demonstrated no age or treatment group changes in total tau levels (HT7; 72 kDa band) (Fig. 6A, B). Therefore, we concluded that total tau expression and distribution were independent of the tau isoform expressed. Immunohistochemical labeling of young adult and middle-aged AAV9-empty capsid-injected mice revealed undetectable total tau levels compared to

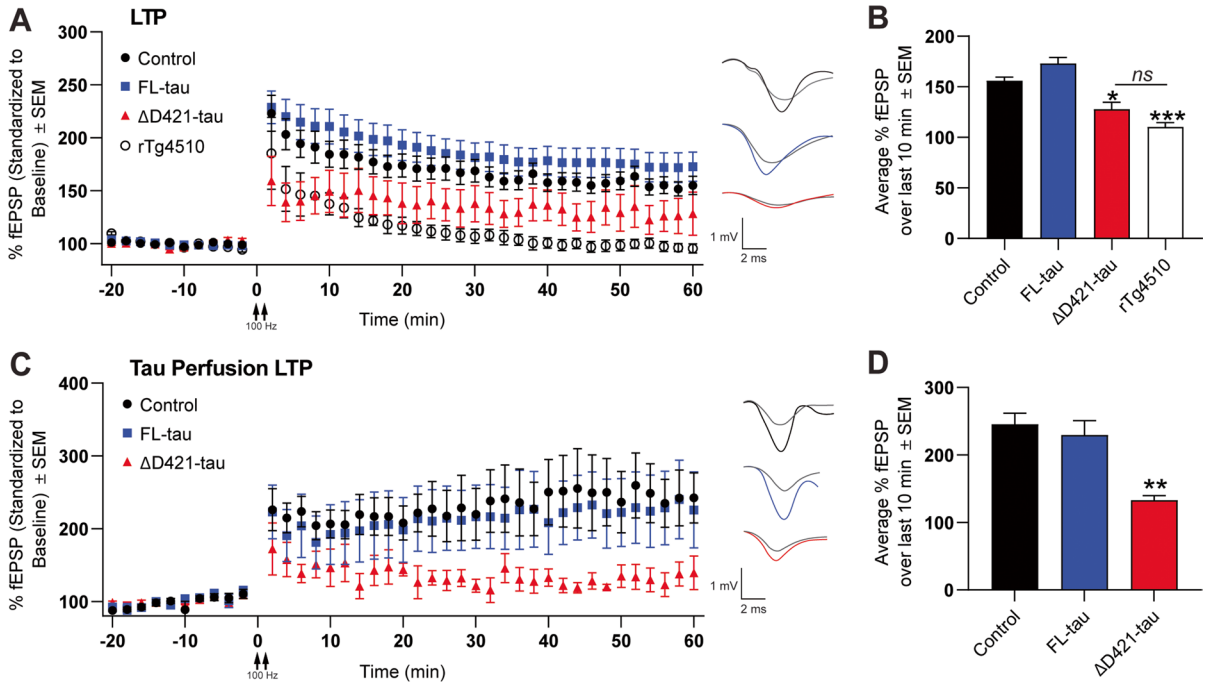

Fig. 4 ΔD421-tau attenuates hippocampal late long-term potentiation (LTP) in middle-aged mice. **A** Attenuated LTP in the hippocampus of middle-aged FL-tau (blue) and ΔD421-tau (red) mice compared with control (black). Hippocampal slices from the transgenic rTg4510 mouse model were used as positive control. **B** Representative fEPSPs recorded in the last 10 min are graphed. Statistical analysis was performed by one-way ANOVA followed by Tukey post-hoc test (n = 4 animal/group, *p < 0.05, **p < 0.01). **C** Impaired LTP induction in middle-aged hippocampal slices perfused with recombinant ΔD421-tau compared with slices perfused with FL-tau or control. **D** Representative fEPSPs recorded in the last 10 min are graphed. Statistical analysis was performed by one-way ANOVA followed by Tukey post-hoc test (n = 4 animal/group, **p < 0.01)

the tau-transduced mice (data not shown); hence, this group was excluded from phosphorylated tau (p-tau) analysis.

Within the young adult mouse cohort, immunohistochemical analysis of HPC and SBC p-tau levels at either serine 396 (pS396) (Fig. 5C, D) or serine 202/threonine 205 (S202/T205; AT8) (Fig. 5E, F) did not differ between FL-tau- and ΔD421-tau-overexpressing mice. In contrast, we observed a significant increase in AT8 levels in middle-aged ΔD421-tau mice compared to the middle-aged cohorts across all measured regions (Fig. 5E, F; Fig. s4E, F). The pS396 levels showed a significant reduction in SBC, and similar trends were found in the HPC of the middle-aged ΔD421-tau mice compared to the middle-aged FL-tau cohort (Fig. 5C, D). Analysis of the CX revealed similar findings for pS396 (Fig. s4C, D).

Western blot analysis revealed that pS396 levels (normalized to total tau, HT7 antibody) were similarly reduced in middle-aged ΔD421-tau mice compared to the middle-aged FL-tau mice (Fig. 6A, B). Further, biochemical analyses revealed that p-tau levels measured by PHF1 and AT180 antibodies in the soluble fraction were significantly increased in the middle-aged FL-tau mice compared to the young adult FL-tau mice. However, this age-associated increase was not evident in the tau soluble fraction from middle-aged ΔD421-tau mice (Fig. 6B). Conversely, we found that pS199-202 tau levels were significantly increased in both young adult and middle-aged ΔD421-tau mice compared to age-matched FL-tau mice.

Next, we investigated insoluble tau levels utilizing a formic acid protocol as previously established [15, 63]. While total tau levels in the insoluble fraction remained unchanged (although higher levels were observed in the aged FL-tau mice), we found a significant increase in pS396 levels in the middle-aged

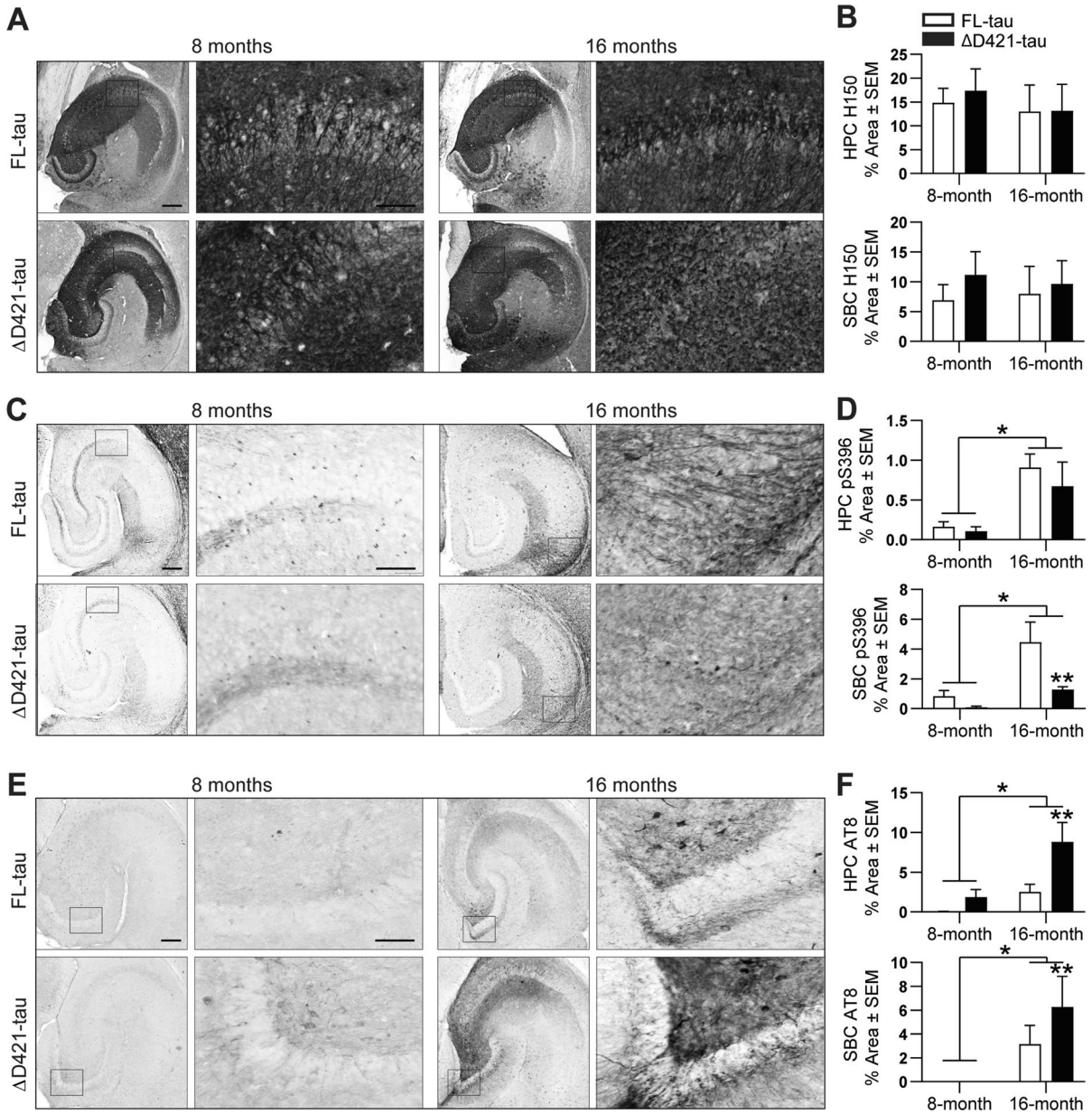

Fig. 5 Differential immunohistochemical phosphorylation profile of FL-tau and ΔD421-tau with age. **A** Immunohistochemical staining of brain tissue for total tau (H150) in the HPC of young adult and middle-aged FL-tau and ΔD421-tau mice. **B** Quantification of percent positive area in the HPC and SBC of young adult and middle-aged FL-Tau- and ΔD421-tau-injected mice. Statistical analyses were performed by two-way ANOVA followed by Tukey post-hoc test (n = 7–8 animal/group). **C** Immunohistochemical staining of brain tissue for phosphorylated S396 levels in the HPC of young adult and middle-aged FL-tau and ΔD421-tau mice. **D** Quantification of percent positive area in HPC and SBC of FL-tau and ΔD421-tau mice. Statistical analyses were carried out by two-way ANOVA followed by Tukey post-hoc test (n = 7–8 animal/group, *$p < 0.05$, **$p < 0.01$). **E** Immunohistochemical staining of brain tissue for phosphorylated S199/Thr205 levels (AT8 antibody). **F** Quantitative analyses of percent positive area in the HPC and SBC of FL- and ΔD421-tau mice. For each marker, statistical analyses were performed by two-way ANOVA followed by Tukey post-hoc test (n = 7–8 animal/group, *$p < 0.05$, **$p < 0.01$). Scale bars represent 200 μm and 20 μm

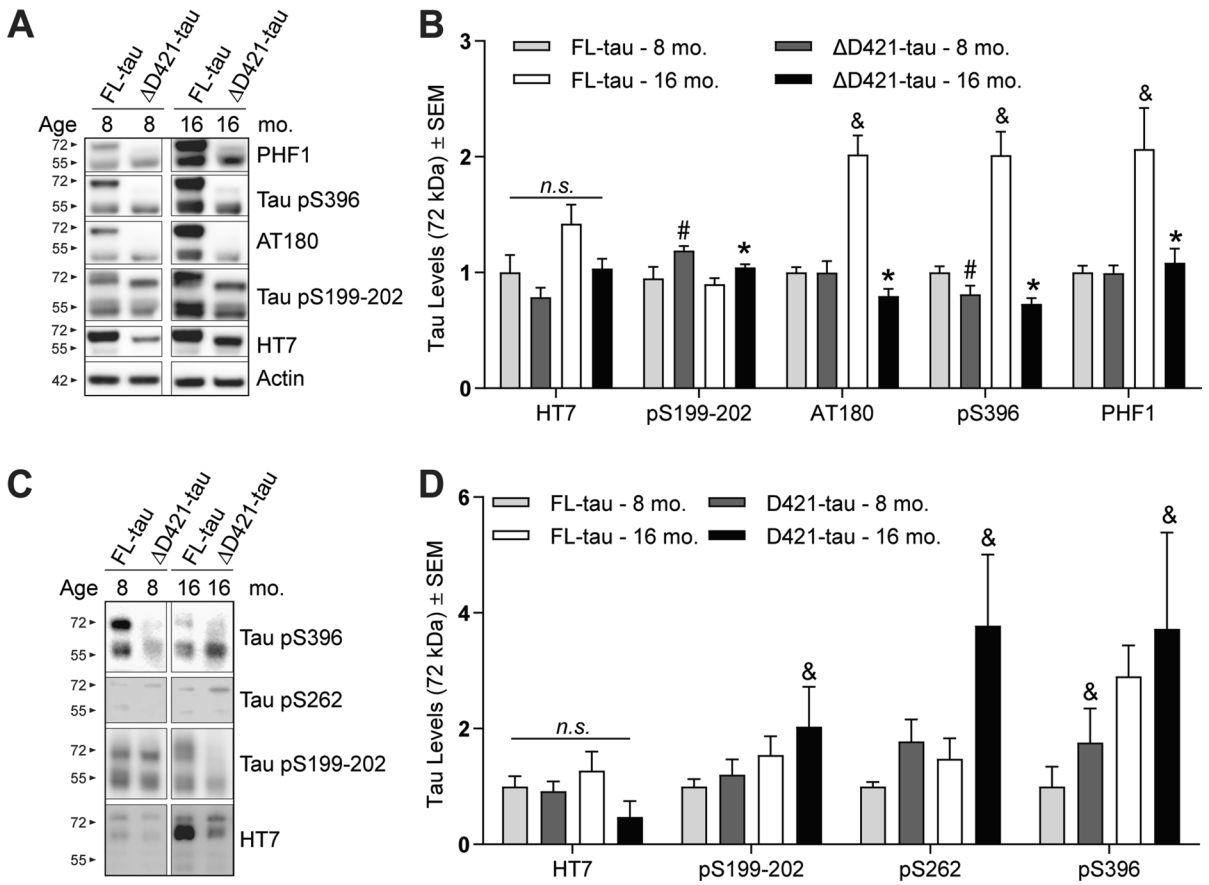

Fig. 6 Differential biochemical phosphorylation profile of FL-tau and ΔD421-tau with age. **A** Representative western blot analysis of the hippocampal RIPA soluble fraction homogenate analyzed for soluble tau levels using total human tau (HT7) and phospho-tau epitopes PHF1 (pS396-404), pS396, AT180 (Thr231), and pS199-202. **B** Band densitometry analysis of total and phosphorylated tau (72 kDa band) in FL-Tau and ΔD421-tau mice. Statistical analyses were performed by two-way ANOVA followed by Tukey post-hoc test (n = 4 animal/group, #p < 0.05 between young adult FL- and ΔD421-tau mice, &p < 0.05 between young adult and middle-aged treatment-matched group, *p < 0.05 between middle-aged FL- and ΔD421-tau mice). **C** Formic acid treated hippocampal fraction (detergent insoluble fraction) was probed for HT7 and phospho-tau epitopes pS396, pS262, and pS199-202. (D) Band densitometry analysis in FL-tau and ΔD421-tau mice. For each fraction, statistical analyses were performed by two-way ANOVA followed by Tukey post-hoc test (n = 5 animal/group, #p < 0.05 between young adult FL- and ΔD421-tau mice, &p < 0.05 between young adult and middle-aged treatment-matched group, *p < 0.05 between middle-aged FL- and ΔD421-tau mice)

FL-tau and ΔD421-tau mice compared to the young adult groups (Fig. 6C, D). P-tau levels at pS262 and pS199-202 epitopes increased in the middle-aged compared to the young adult ΔD421-tau group, but not in the FL-tau groups independent of age (Fig. 6C, D). Overall, these results show that FL-tau and ΔD421-tau result in distinct phosphorylation profiles in middle-aged mice.

Oligomeric tau formation is enhanced in middle-aged ΔD421-tau-overexpressing mice

Next, we performed Gallyas silver staining in both age cohorts to assess silver-positive tangle pathology and found significant increases in argyrophilic tau in both the middle-aged FL-tau and ΔD421-tau mice compared to the young adult groups (Fig. 7A, B). Quantification of the percentage of the positive area also revealed regional differences between ΔD421-tau and FL-tau mice. For example,

middle-aged ΔD421-tau mice exhibited significantly lower argyrophilic tau levels in the cortex compared to age-matched FL-tau mice (Fig. s5A, B), while argyrophilic tau levels in the HPC or SBC did not differ between middle-aged FL-tau and ΔD421-tau mice (Fig. 7A, B).

A dot blot assay with T22 oligomeric antibody demonstrated increased tau oligomer levels in the middle-aged FL-tau and ΔD421-tau mice compared to the young adult groups (Fig. 7C, D). Notably, the middle-aged ΔD421-tau mice developed significantly more tau oligomers in the hippocampus compared to middle-aged FL-tau mice (Fig. 7C, D). These data collectively suggest that while age is important contributing factor to FL-tau and ΔD421-tau oligomer and silver-positive tangle formation, ΔD421-tau is more prone to oligomerization in the aging brain while displaying less aggregate/tangle formation in vivo.

Tau pathology induced neurodegeneration in middle-aged FL-tau and ΔD421-tau mice

Because of the behavioral, biochemical, and electrophysiological differential profiles of FL-tau and ΔD421-tau, we investigated the impact of the tau pathology on neuronal loss using the NeuN neuronal marker. We observed reduced NeuN neuronal labeling in the HPC of middle-aged FL-tau and ΔD421-tau mice following tau accumulation and phosphorylation compared to age-matched controls (Fig. 8A, B). Young adult mouse groups showed no difference in NeuN labeling of neurons. Additional analysis of the CA3 region of the HPC in the middle-aged FL-tau and ΔD421-tau mice, the targeted region for stereotaxic injections, demonstrated increased toxicity of ΔD421-tau to CA3 pyramidal neurons (Fig. 8C). To further dissect differences in neuronal loss, we measured NeuN-positive area in the synaptically connected SBC region, previously showing viral transduction (Fig. 1B, C), and found no neuronal loss between the FL-tau and ΔD421-tau mice (Fig. 8D). In-depth analyses of the CX showed

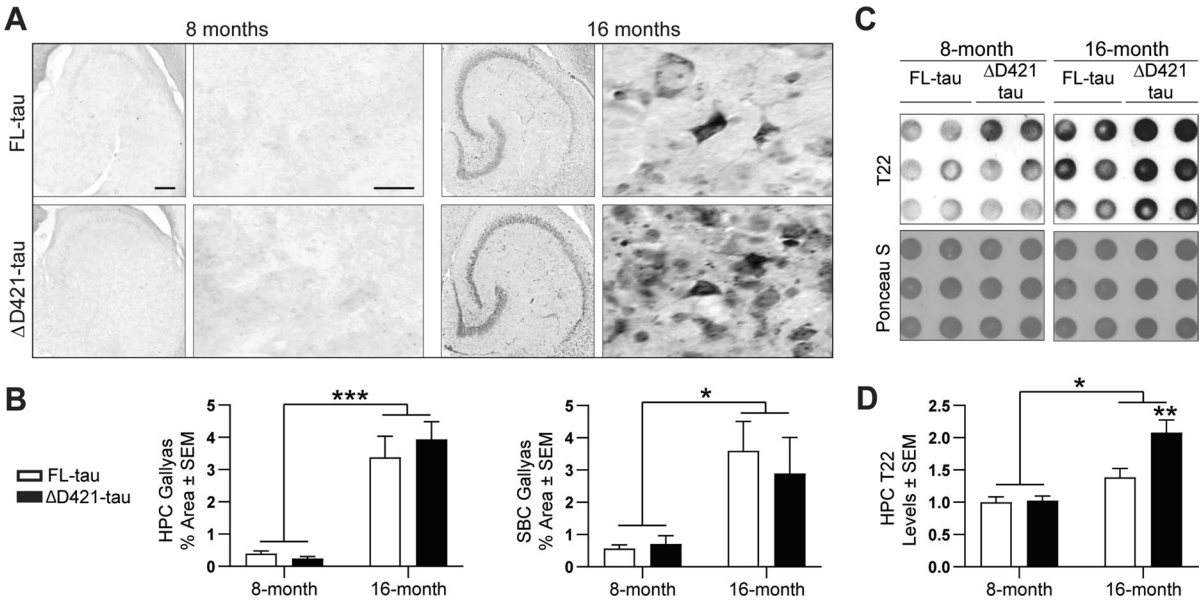

Fig. 7 Deposition of FL-tau and ΔD421-tau into silver-positive and oligomeric forms. **A** The Gallyas histology of the HPC of FL-tau and ΔD421-tau mice. **B** Quantitative analysis of argyrophilic tau density in the HPC and SBC of FL-tau and ΔD421-tau mice. Statistical analyses were performed by two-way ANOVA with Tukey post-hoc test (n = 7–8 animal/group, *p < 0.05, ***p < 0.001). Scale bars represent 200 μm and 20 μm. **C** Dot blot analysis of the soluble tau fraction for oligomeric tau levels in the hippocampal homogenate. **D** Dot blot densitometry analysis of oligomeric tau levels. Statistical analyses were performed by one-way ANOVA with Tukey post-hoc test (n = 6 animal/group, **p < 0.01)

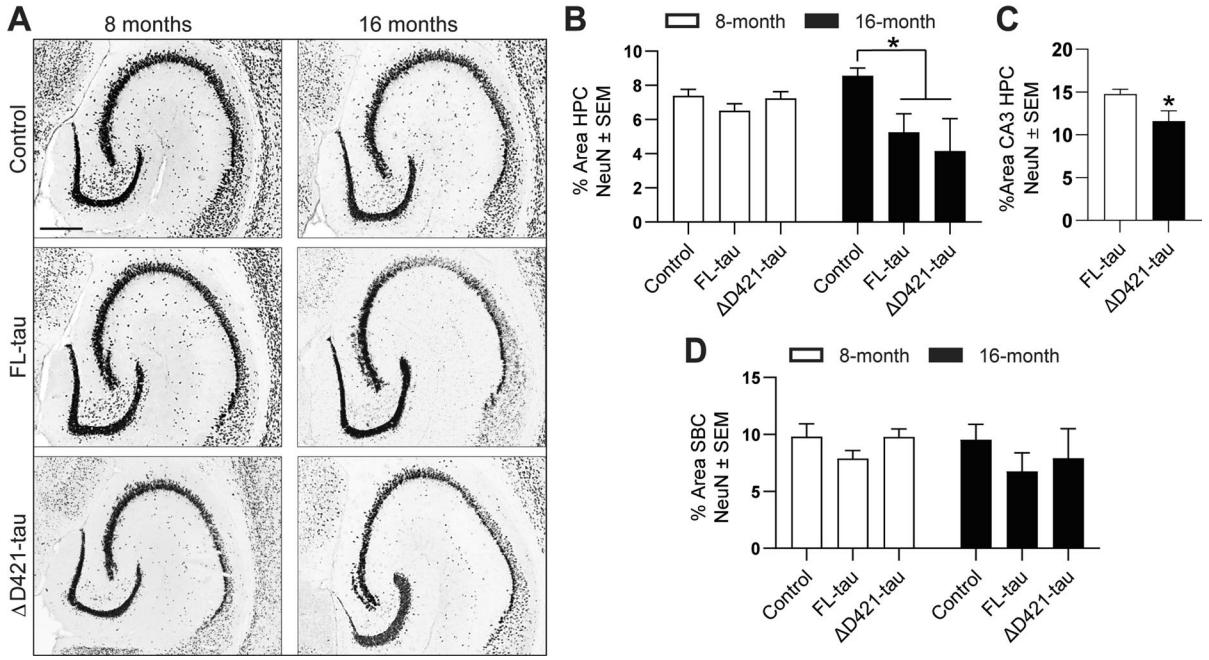

Fig. 8 Overexpression of FL-tau and ΔD421-tau promotes neuronal degeneration in middle-aged mice. **A** Micrographs from NeuN stain from the hippocampi of mice receiving AAV9-empty capsid, FL-tau and ΔD421-tau. **B** Quantification of the NeuN intensity in the HPC of FL-tau and ΔD421-tau mice. Statistical analyses were performed by two-way ANOVA followed by Tukey post-hoc test (n = 7–8 animal/group, *p < 0.05, **p < 0.01, ***p < 0.001. **C** Quantification of the NeuN intensity in the CA3 region of the HPC of middle-aged FL-tau and ΔD421-tau mice. Statistical analysis was performed by Student's t-test (n = 7–8 animal/group, *p < 0.05). **D** Quantification of the NeuN intensity in the SBC of FL-tau and ΔD421-tau mice. Statistical analysis was performed by Student's *t* test (n = 7–8 animal/group). Scale bar represents 200 µm

extensive neurodegeneration in middle-aged FL- and ΔD421-tau mice compared to age-matched controls, with no neuronal loss observed in the corresponding young adult groups (Fig. s6). Interestingly, age alone did not affect neuronal density in the control animal cohort.

To further investigate the marked neuronal loss in the entorhinal cortex, we assessed NeuN immunoreactivity in the medial (MEC) and lateral entorhinal cortex EC (LEC) subregions. Neuronal inputs and outputs from layer II/III of the MEC and LEC are of particular interest in interpreting the behavioral outcomes as they inform the hippocampus on spatial or sensory information, respectively (Fig. 9A) [42]. We demonstrated a significant neuronal loss in the MEC following ΔD421-tau expression in middle-aged mice, while both FL-tau and ΔD421-tau induced significant neuronal loss in LEC (Fig. 9B, C). Similarly, ΔD421-tau expression caused marked layer II/ III cortical thinning of the MEC, while both tau forms affected LEC region thickness (Fig. 9C). Altogether our data suggest increased regional toxicity of ΔD421-tau species compared to FL-tau, possibly due to its tendency to oligomerize and its differential phosphorylation pattern. We summarized the neuropathological phenotypes associated with FL-tau and ΔD421-tau overexpression in mice in Table 1.

Discussion

Caspase cleavage of tau at D421 is considered an early event in AD pathology and is associated with neurodegeneration and tangle formation in other transgenic models [56, 80]. Our study reports that accumulation of tau truncated at D421 in middle-aged, but not in young adult mice, can differentially worsen cognition, synaptic plasticity, and regional neurodegeneration compared to FL-tau. Hence, in addition to revealing a differential effect of D421 tau, this study sheds

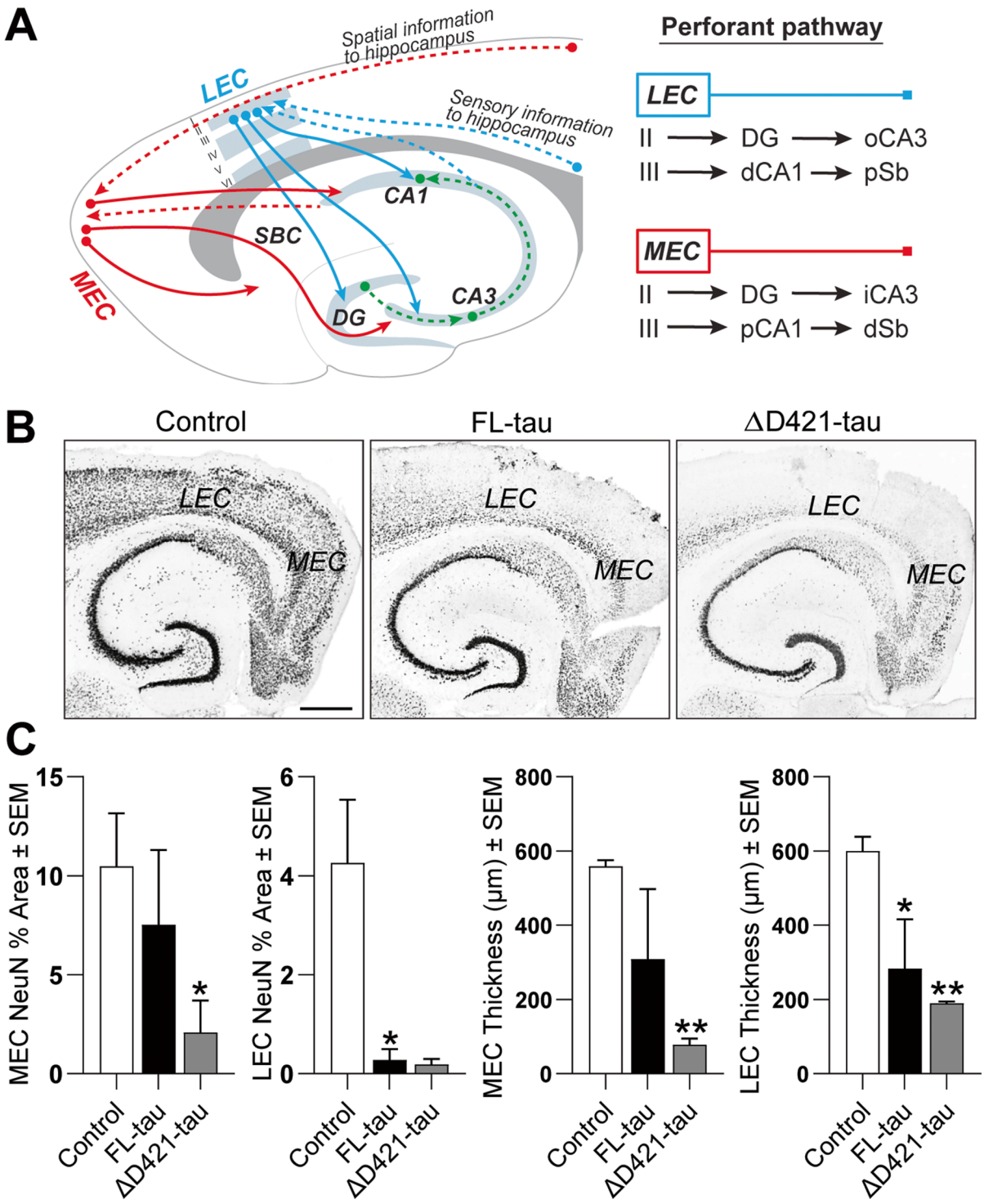
A
Spatial information to hippocampus
Sensory information to hippocampus
LEC
MEC
I
II
III
IV
V
VI
CA1
SBC
DG
CA3
Perforant pathway
LEC
II → DG → oCA3
III → dCA1 → pSb
MEC
II → DG → iCA3
III → pCA1 → dSb
B
Control
FL-tau
ΔD421-tau
LEC
MEC
C
MEC NeuN % Area ± SEM
LEC NeuN % Area ± SEM
MEC Thickness (μm) ± SEM
LEC Thickness (μm) ± SEM
Control
FL-tau
ΔD421-tau

◂ **Fig. 9** FL-tau and ΔD421-tau pathology induces lateral (LEC) and medial entorhinal cortex (MEC) degeneration. **A** Schematic presentation of the anatomical characteristics of hippocampal-entorhinal trisynaptic perforant pathway. Cortical inputs from LEC and MEC to the hippocampus carry different sensory and spatial information, respectively. **B** NeuN immunohistochemical detection on brain tissue from middle-aged mice receiving empty capsid (control), FL-tau or ΔD421-tau. **C** Percent NeuN-positive area and thickness of layer II/III of the LEC and MEC subfields in middle-aged FL-tau and ΔD421-tau mice compared to age-matched empty capsid control group. Statistical analyses were performed by one-way ANOVA followed by Tukey post-hoc test (n = 7–8 animal/group, *$p < 0.05$, **$p < 0.01$). LEC, lateral entorhinal cortex; MEC, medial entorhinal cortex, DG, dentate gyrus, oCA3, outer molecular layer of CA3, iCA3, inner molecular layer of CA3, dCA1, distal CA1, pCA1, proximal CA1, dSb, distal subiculum, pSb, proximal subiculum. Scale bar represents 500 μm

light on the impact of age on the brain's susceptibility to damage from the accumulation of AD-associated tau species. As the most significant risk factor for AD, normal aging brings forth molecular and cellular alterations to the neural milieu, such as changes in DNA methylation and histone acetylation, glial pro-inflammatory phenotypes, accumulation of reactive oxygen species, and impaired autophagy, each of which can contribute to the accumulation and toxicity of tau species [78]. For example, miRNA-219 regulates tau hyperphosphorylation and is negatively regulated in AD [31, 58, 59], while deletion of macroautophagy-related factor Atg7 leads to premature aging and induced tau phosphorylation [32]. As we have previously reported, neuroinflammation promotes tau hyperphosphorylation [35, 44]. Aging can also alter neurotransmission such as decreased neuronal excitability and calcium dysregulation [24, 50]. Moreover, previous studies have hypothesized that the aged brain environment is more conducive to tau-induced pathology [72]. In this work, we sought to investigate species-specific differences in FL-tau- and ΔD421-tau-induced pathologies and found significant differences in middle-aged mice that were largely absent in young adult mice. Still, while the effect of differing age is essential to our findings, the specific conditions in aging under which tau can exert neurotoxic effects should be further investigated and defined by future experimentation.

With respect to our study, we provide evidence that middle-aged ΔD421-tau mice exhibited impaired long-term memory both in the fear conditioning and radial arm water maze tasks coupled with LTP disturbance, effects that were absent in the age-matched FL-tau mice. These data support a role for ΔD421-tau in synaptic plasticity, especially since ΔD421-tau is enriched in the cortical pre-synaptic compartment of AD brains [65]. To this end, we showed that hippocampal ΔD421-tau overexpression corresponded with downregulation in the mRNA of several genes (*Mmp9*, *Bdnf*, and *Adcy8*), which could play a synergistic role in ΔD421-tau-dependent LTP deficits. Indeed, studies have demonstrated that knock-out of the corresponding proteins for the above genes impaired LTP [28, 46, 73]. Previous literature also describes how tau-synaptic interactions could be differentially altered by cleavage at D421. For example, endogenous tau has been shown to interact with synapses at the PSD95-NMDA receptor complex [49]. Further, mice lacking NMDARs in connected hippocampal regions display similar behavioral deficits found in our study, where spatial reversal learning is impaired [9, 68], indicating potential alternative pathways affected by ΔD421-tau. Interestingly, preventing ΔD421-tau cleavage also results in impaired LTP maintenance and performance in the Morris water maze, which could indicate that a homeostatic flux in tau cleavage is important for learning and memory [12]. Therefore, further research directed at understanding the molecular underpinnings behind tau-mediated synaptic plasticity alterations is necessary to understand the physiological function of tau cleavage.

We examined tau phosphorylation patterns in mice to better understand how ΔD421-tau protein is involved in synaptic and behavioral changes. Biochemical analysis of soluble tau demonstrated significant induction of hippocampal AT180, pS396, and PHF1 tau levels in the middle-aged FL-tau that were suppressed in ΔD421-tau mice. This is consistent with a previous report demonstrating that ΔD421-tau is not as efficiently phosphorylated by GSK3β [18], suggesting the possibility that tau truncation alters interactions with specific kinases. Interestingly, AT8 immunoreactivity was induced in middle-aged ΔD421-tau mice. The extent of cytotoxicity of phosphorylated tau and its role in tau dynamics is still a topic of debate,yet mounting evidence identifies tau oligomerization as a toxic entity associated with tau seeding, misfolding, propagation, loss of synapses, and calcium-induced apoptotic pathways [33, 36, 71]. Notably, oligomeric tau levels were significantly

Table 1 Summary of findings in the study with respect to age (16 months versus 8 months) and treatment (ΔD421-tau versus FL-tau)

Measure	16 months vs. 8 months		ΔD421-tau vs. FL-tau	
	FL-tau	ΔD421-tau	8 months	16 months
Spatial memory	↓	↓	-	↓↓
LTP				↓
Fear memory				
Context				↓
Cued				↓
Neuronal loss	↓	↓	-	↓
Phosphorylation				
AT8	↑	↑	↑	↑↑
pS396	↑	↑	↓	↓↓
PHF1	↑	-	-	↓
pS199-202	-	-	↑	↑
Gallyas	↑	↑	-	↓
Oligomerization	↑	↑	-	↑↑
T22				

Up arrow (↑) indicates an increase, while the down arrow (↓) indicates a decrease in the selected measure

increased in middle-aged ΔD421-tau mice relative to age-matched FL-tau mice. The enhanced ΔD421-tau oligomer formation could play an essential role in regional neurodegeneration and synaptic and behavioral deficits. For example, studies show that tau oligomerization can increase neuronal loss and RAWM memory deficits, while decreasing tau oligomerization has been shown to prevent both [7, 64]. Further, tau oligomer administration into mouse hippocampi impaired fear memory and reduced LTP in previous studies [22], while specific inhibition of caspase-cleaved tau oligomer formation improved memory in several neurobehavioral tasks [41]. Altogether, these reports support our notion that oligomerization of ΔD421-tau could contribute to the behavioral impairments we observed in middle-aged mice.

In addition to hippocampal neuronal toxicity, we also identified the MEC as an exceptionally vulnerable region to overexpression of ΔD421-tau in aged mice, demonstrated by shrinkage of the superficial layer II/III and reduced NeuN-positive area. This effect could be due to tau spreading or increased viral transduction into the entorhinal cortex, as elegantly studied elsewhere [19, 38, 77]. Our study, however, was designed to understand species-specific tau pathology and not the propagation of specific tau isoforms. To this point, we demonstrated selective susceptibility of MEC neurons toward ΔD421-tau toxicity. As layer II/III of the MEC is part of the perforant pathway's classical trisynaptic (ECII → dentate gyrus → CA3 → CA1) and monosynaptic circuits (ECIII → CA1) with differential neuronal inputs in hippocampus mediating memory formation [42], our findings could represent another avenue by which ΔD421-tau contributes to the spatial memory impairments observed with age in this model. One possible mechanism to this vulnerability could be the reported tonically active pre-synaptic NMDARs present in the EC that can aberrantly increase calcium-dependent glutamate release, activating apoptotic factors [11, 45, 75].

Overall, our studies highlight the effect of FL- and ΔD421-tau accumulation on cognitive impairment and neuronal loss in middle-aged mice. While age alone can heighten susceptibility to tau-induced damaging effects, we showed that increased ΔD421-tau levels contribute to deficits in synaptic plasticity and cognitive impairments in the aged brain milieu. Given its oligomeric and phosphorylation profile revealed here, we propose a novel ΔD421-tau pathological signature that can contribute to disease progression in aged individuals and AD patients. Future studies aimed at understanding tau cleavage dynamics and mechanisms leading to ΔD421 accumulation with age can be of therapeutic interest for AD and other tauopathies.

Author contribution Conceptualization: M.L.B.S, M.N.G., and D.M. Methodology: M.L.B.S. Formal analysis: MLBS, AL, FZ, AS, and ZQ. Investigation: AL, FZ, AS, BB, SS, MLB, ZQ, and MP. Resources: MLBS, DCL, EW, KN, MNG, and DM. Writing–original draft: MLBS. Writing–review and editing: MLBS, AL, FZ, and MNG. Visualization: MLBS, AL, and FZ. Supervision: MLBS. Funding Acquisition: MLBS, MNG, and DM.

Funding This work was supported by Seed Grant funds from the College of Pharmacy, Byrd Alzheimer's Institute at the University of South Florida, and NIH grant R01 AG 051500 to DGM.

Data availability All relevant data are available upon request directed to the corresponding author.

Declarations

Ethics approval Animal procedures were performed in accordance with the recommendations of the National Research Council's "Guide for the Care and Use of Laboratory Animals" and were previously approved by the University of South Florida Institute of Animal Care and Use Committee (IACUC).

Consent for publication Not applicable.

Conflict of interest The authors declare no competing interests.

References

1. Abisambra J, Jinwal UK, Miyata Y, Rogers J, Blair L, Li X, Seguin SP, Wang L, Jin Y, Bacon J, Brady S, Cockman M, Guidi C, Zhang J, Koren J, Young ZT, Atkins CA, Zhang B, Lawson LY, Weeber EJ, Brodsky JL, Gestwicki JE, Dickey CA. Allosteric heat shock protein 70 inhibitors rapidly rescue synaptic plasticity deficits by reducing aberrant tau. Biol Psychiatry. 2013. https://doi.org/10.1016/j.biopsych.2013.02.027
2. Abraha A, Ghoshal N, Gamblin TC, Cryns V, Berry RW, Kuret J, Binder LI. C-terminal inhibition of tau assembly in vitro and in Alzheimer's disease. J Cell Sci. 2000. https://doi.org/10.1242/jcs.113.21.3737
3. Adalbert R, Gilley J, Coleman MP. Aβ, tau and ApoE4 in Alzheimer's disease: the axonal connection. Trends Mol Med. 2007. https://doi.org/10.1016/j.molmed.2007.02.004.
4. Ahmed Z, Cooper J, Murray TK, Garn K, McNaughton E, Clarke H, Parhizkar S, Ward MA, Cavallini A, Jackson S, Bose S, Clavaguera F, Tolnay M, Lavenir I, Goedert M, Hutton ML, O'Neill MJ. A novel in vivo model of tau propagation with rapid and progressive neurofibrillary tangle pathology: The pattern of spread is determined by connectivity, not proximity. Acta Neuropathol. 2014. https://doi.org/10.1007/s00401-014-1254-6.
5. Alamed J, Wilcock DM, Diamond DM, Gordon MN, Morgan D. Two-day radial-arm water maze learning and memory task; robust resolution of amyloid-related memory deficits in transgenic mice. Nat Protoc. 2006. https://doi.org/10.1038/nprot.2006.275.
6. Allen. ALLEN Mouse Brain Atlas. Gene Expr. 2007. https://doi.org/10.1038/nature05453.
7. Baker JD, Shelton LB, Zheng D, Favretto F, Nordhues BA, Darling A, Sullivan LE, Sun Z, Solanki PK, Martin MD, Suntharalingam A, Sabbagh JJ, Becker S, Mandelkow E, Uversky VN, Zweckstetter M, Dickey CA, Koren J, Blair LJ. Human cyclophilin 40 unravels neurotoxic amyloids. PLoS Biol. 2017. https://doi.org/10.1371/journal.pbio.2001336.
8. Bancher C, Brunner C, Lassmann H, Budka H, Jellinger K, Wiche G, Seitelberger F, Grundke-Iqbal I, Iqbal K, Wisniewski HM. Accumulation of abnormally phosphorylated τ precedes the formation of neurofibrillary tangles in Alzheimer's disease. Brain Res. 1989. https://doi.org/10.1016/0006-8993(89)91396-6.
9. Bannerman DM, Bus T, Taylor A, Sanderson DJ, Schwarz I, Jensen V, Hvalby Ø, Rawlins JNP, Seeburg PH, Sprengel R. Dissecting spatial knowledge from spatial choice by hippocampal NMDA receptor deletion. Nat Neurosci. 2012;15(8):1153–9. https://doi.org/10.1038/nn.3166.
10. Basurto-Islas G, Luna-Muñoz J, Guillozet-Bongaarts AL, Binder LI, Mena R, García-Sierra F. Accumulation of aspartic acid421- and glutamic acid 391-cleaved tau in neurofibrillary tangles correlates with progression in Alzheimer disease. J Neuropathol Exp Neurol. 2008. https://doi.org/10.1097/NEN.0b013e31817275c7.
11. Berretta N, Jones RSG. Tonic facilitation of glutamate release by pre-synaptic N-methyl-D-aspartate autoreceptors in the entorhinal cortex. Neuroscience. 1996;75(2):339–44. https://doi.org/10.1016/0306-4522(96)00301-6.
12. Biundo F, d'Abramo C, Tambini MD, Zhang H, Del Prete D, Vitale F, Giliberto L, Arancio O, D'Adamio L. Abolishing Tau cleavage by caspases at Aspartate421 causes memory/synaptic plasticity deficits and pre-pathological Tau alterations. Transl Psychiatry. 2017. https://doi.org/10.1038/tp.2017.165.
13. Brownlow ML, Joly-Amado A, Azam S, Elza M, Selenica ML, Pappas C, Small B, Engelman R, Gordon MN, Morgan D. Partial rescue of memory deficits induced by calorie restriction in a mouse model of tau deposition. Behav Brain Res. 2014. https://doi.org/10.1016/j.bbr.2014.06.001.
14. Carmel G, Mager EM, Binder LI, Kuret J. The structural basis of monoclonal antibody Alz50's selectivity for Alzheimer's disease pathology. J Biol Chem. 1996. https://doi.org/10.1074/jbc.271.51.32789.
15. Carroll JC, Iba M, Bangasser DA, Valentino RJ, James MJ, Brunden KR, Lee VMY, Trojanowski JQ. Chronic stress exacerbates tau pathology, neurodegeneration, and cognitive performance through a corticotropin-releasing factor receptor-dependent mechanism in a transgenic mouse model of tauopathy. J Neurosci. 2011. https://doi.org/10.1523/JNEUROSCI.3836-11.2011.
16. Carty N, Lee D, Dickey C, Ceballos-Diaz C, Jansen-West K, Golde TE, Gordon MN, Morgan D, Nash K. Convection-enhanced delivery and systemic mannitol increase gene product distribution of AAV vectors 5, 8, and 9 and increase gene product in the adult mouse brain. J Neurosci Methods. 2010. https://doi.org/10.1016/j.jneumeth.2010.10.010.
17. Chai X, Dage JL, Citron M. Constitutive secretion of tau protein by an unconventional mechanism. Neurobiol Dis. 2012. https://doi.org/10.1016/j.nbd.2012.05.021.
18. Cho JH, Johnson GVW. Glycogen synthase kinase 3β induces caspase-cleaved tau aggregation in situ. J Biol Chem. 2004. https://doi.org/10.1074/jbc.M403364200.
19. Clavaguera F, Grueninger F, Tolnay M. Intercellular transfer of tau aggregates and spreading of tau pathology: implications for therapeutic strategies. Neuropharmacology. 2014. https://doi.org/10.1016/j.neuropharm.2013.08.037.
20. De Calignon A, Polydoro M, Suárez-Calvet M, William C, Adamowicz DH, Kopeikina KJ, Pitstick R, Sahara N, Ashe KH, Carlson GA, Spires-Jones TL, Hyman BT. Propagation of tau pathology in a model of early

Alzheimer's disease. Neuron. 2012. https://doi.org/10.1016/j.neuron.2011.11.033.
21. Drubin DG, Kirschner MW. Tau protein function in living cells. J Cell Biol. 1986. https://doi.org/10.1083/jcb.103.6.2739.
22. Fá M, Puzzo D, Piacentini R, Staniszewski A, Zhang H, Baltrons MA, Li Puma DD, Chatterjee I, Li J, Saeed F, Berman HL, Ripoli C, Gulisano W, Gonzalez J, Tian H, Costa JA, Lopez P, Davidowitz E, Yu WH, Haroutunian V, Brown LM, Palmeri A, Sigurdsson EM, Duff KE, Teich AF, Honig LS, Sierks M, Moe JG, D'Adamio L, Grassi C, Kanaan NM, Fraser PE, Arancio O. Extracellular tau oligomers produce an immediate impairment of ltp and memory. Sci Rep. 2016. https://doi.org/10.1038/srep19393.
23. Flurkey K, Currer JM, Harrison DE. Mouse models in aging research. In: Fox J, Barthold S, Davisson M, Newcomer C, Quimby F, Smith A. The Mouse in Biomedical Research. Vol. 3. Elsevier Inc; 2007. pp. 637–672. https://doi.org/10.1016/B978-012369454-6/50074-1.
24. Foster TC, Norris CM. Age-associated changes in Ca2+-dependent processes: Relation to hippocampal synaptic plasticity. Hippocampus. 1997;7(6):602–12. https://doi.org/10.1002/(SICI)1098-1063(1997)7:6%3c602::AID-HIPO3%3e3.0.CO;2-G.
25. Frost B, Diamond MI. Prion-like mechanisms in neurodegenerative diseases. Nat Rev Neurosci. 2010. https://doi.org/10.1038/nrn2786.
26. Gamblin TC, Chen F, Zambrano A, Abraha A, Lagalwar S, Guillozet AL, Lu M, Fu Y, Garcia-Sierra F, LaPointe N, Miller R, Berry RW, Binder LI, Cryns VL. Caspase cleavage of tau: Linking amyloid and neurofibrillary tangles in Alzheimer's disease. Proc Natl Acad Sci USA. 2003. https://doi.org/10.1073/pnas.1630428100.
27. García-Sierra F, Mondragón-Rodríguez S, Basurto-Islas G. Truncation of tau protein and its pathological significance in Alzheimer's disease. J Alzheimers Dis. 2008. https://doi.org/10.3233/JAD-2008-14407.
28. Gorkiewicz T, Balcerzyk M, Kaczmarek L, Knapska E. Matrix metalloproteinase 9 (MMP-9) is indispensable for long term potentiation in the central and basal but not in the lateral nucleus of the amygdala. Front Cell Neurosci. 2015;9:73. https://doi.org/10.3389/fncel.2015.00073.
29. Greenberg SG, Davies P. A preparation of Alzheimer paired helical filaments that displays distinct τ proteins by polyacrylamide gel electrophoresis. Proc Natl Acad Sci USA. 1990. https://doi.org/10.1073/pnas.87.15.5827.
30. Guo H, Albrecht S, Bourdeau M, Petzke T, Bergeron C, LeBlanc AC. Active caspase-6 and caspase-6-cleaved tau in neuropil threads, neuritic plaques, and neurofibrillary tangles of Alzheimer's disease. Am J Pathol. 2004. https://doi.org/10.1016/S0002-9440(10)63317-2.
31. Hernandez-Rapp J, Rainone S, Goupil C, Dorval V, Smith PY, Saint-Pierre M, Vallée M, Planel E, Droit A, Calon F, Cicchetti F, Hébert SS. MicroRNA-132/212 deficiency enhances Aβ production and senile plaque deposition in Alzheimer's disease triple transgenic mice. Sci Rep. 2016;6(1):1–11. https://doi.org/10.1038/srep30953.
32. Inoue K, Rispoli J, Kaphzan H, Klann E, Chen EI, Kim J, Komatsu M, Abeliovich A. Macroautophagy deficiency mediates age-dependent neurodegeneration through a phospho-tau pathway. Mol Neurodegener. 2012;7:48. https://doi.org/10.1186/1750-1326-7-48.
33. Jiang L, Ash PEA, Maziuk BF, Ballance HI, Boudeau S, Abdullatif AA, Orlando M, Petrucelli L, Ikezu T, Wolozin B. TIA1 regulates the generation and response to toxic tau oligomers. Acta Neuropathol. 2019;137(2):259–77. https://doi.org/10.1007/s00401-018-1937-5.
34. Jicha GA, Berenfeld B, Davies P. Sequence requirements for formation of conformational variants of tau similar to those found in Alzheimer's disease. J Neurosci Res. 1999. https://doi.org/10.1002/(SICI)1097-4547(19990315)55:6%3c713::AID-JNR6%3e3.0.CO;2-G.
35. Joly-Amado A, Hunter J, Quadri Z, Zamudio F, Rocha-Rangel PV, Chan D, Kesarwani A, Nash K, Lee DC, Morgan D, Gordon MN, Selenica M-LB. CCL2 overexpression in the brain promotes glial activation and accelerates tau pathology in a mouse model of tauopathy. Front Immunol. 2020;11:997. https://doi.org/10.3389/fimmu.2020.00997.
36. Jucker M, Walker LC. Self-propagation of pathogenic protein aggregates in neurodegenerative diseases. Nature. 2013; 501(7465):45-51. https://doi.org/10.1038/nature12481.
37. Kanmert D, Cantlon A, Muratore CR, Jin M, O'Malley TT, Lee G, Young-Pearse TL, Selkoe DJ, Walsh DM. C-terminally truncated forms of tau, but not full-length tau or its C-terminal fragments, are released from neurons independently of cell death. J Neurosci. 2015. https://doi.org/10.1523/JNEUROSCI.0387-15.2015.
38. Kfoury N, Holmes BB, Jiang H, Holtzman DM, Diamond MI. Trans-cellular propagation of tau aggregation by fibrillar species. J Biol Chem. 2012. https://doi.org/10.1074/jbc.M112.346072.
39. Khan UA, Liu L, Provenzano FA, Berman DE, Profaci CP, Sloan R, Mayeux R, Duff KE, Small SA. Molecular drivers and cortical spread of lateral entorhinal cortex dysfunction in preclinical Alzheimer's disease. Nat Neurosci. 2014. https://doi.org/10.1038/nn.3606.
40. Kim WH, Lee S, Hall GF. Secretion of human tau fragments resembling CSF-tau in Alzheimer's disease is modulated by the presence of the exon 2 insert. FEBS Lett. 2010. https://doi.org/10.1016/j.febslet.2010.05.042.
41. Kim YD, Choi H, Lee WJ, Park H, Kam TI, Hong Shoon, Nah J, Jung S, Shin B, Lee H, Choi TY, Choo H, Kim KK, Choi SY, Kayed R, Jung YK. Caspase-cleaved tau exhibits rapid memory impairment associated with tau oligomers in a transgenic mouse model. Neurobiol Dis. 2016. https://doi.org/10.1016/j.nbd.2015.12.006.
42. Knierim JJ, Neunuebel JP, Deshmukh SS. Functional correlates of the lateral and medial entorhinal cortex: objects, path integration and local-global reference frames. Philos Trans R Soc Lond B Biol Sci. 2013;369(1635):20130369. https://doi.org/10.1098/rstb.2013.0369.
43. Lasagna-Reeves CA, Castillo-Carranza DL, Sengupta U, Clos AL, Jackson GR, Kayed R. Tau oligomers impair memory and induce synaptic and mitochondrial dysfunction in wild-type mice. Mol Neurodegener. 2011. https://doi.org/10.1186/1750-1326-6-39.
44. Lee DC, Rizer J, Selenica MLB, Reid P, Kraft C, Johnson A, Blair L, Gordon MN, Dickey CA, Morgan D. LPS-induced inflammation exacerbates phospho-tau pathology

in rTg4510 mice. J Neuroinflammation. 2010;7:56. https://doi.org/10.1186/1742-2094-7-56.
45. Lench AM, Robson E, Jones RSG. Differential effects of D-cycloserine and ACBC at NMDA receptors in the rat entorhinal cortex are related to efficacy at the co-agonist binding site. PLoS ONE. 2015;10(7):e0133548. https://doi.org/10.1371/journal.pone.0133548.
46. Lu Y, Christian K, Lu B. BDNF: a key regulator for protein synthesis-dependent LTP and long-term memory? Neurobiol Learn Mem. 2008;89(3):312–23. https://doi.org/10.1016/j.nlm.2007.08.018.
47. Luna-Muñoz J, Chávez-Macías L, García-Sierra F, Mena R. Earliest stages of tau conformational changes are related to the appearance of a sequence of specific phospho-dependent tau epitopes in Alzheimer's disease. J Alzheimers Dis. 2007. https://doi.org/10.3233/JAD-2007-12410.
48. McMillan PJ, Kraemer BC, Robinson L, Leverenz JB, Raskind M, Schellenberg G. Truncation of tau at E391 promotes early pathologic changes in transgenic mice. J Neuropathol Exp Neurol. 2011. https://doi.org/10.1097/NEN.0b013e31823557fb.
49. Mondragón-Rodríguez S, Trillaud-Doppia E, Dudilot A, Bourgeois C, Lauzon M, Leclerc N, Boehm J. Interaction of endogenous tau protein with synaptic proteins is regulated by N-methyl-D-aspartate receptor-dependent tau phosphorylation. J Biol Chem. 2012. https://doi.org/10.1074/jbc.M112.401240.
50. Oh MM, Oliveira FA, Disterhoft JF. Learning and aging related changes in intrinsic neuronal excitability. Front Aging Neurosci. 2010; 2:2. https://doi.org/10.3389/neuro.24.002.2010
51. Park SY, Ferreira A. The generation of a 17 kDa neurotoxic fragment: An alternative mechanism by which tau mediates β-amyloid-induced neurodegeneration. J Neurosci. 2005;25(22):5365–75. https://doi.org/10.1523/JNEUROSCI.1125-05.2005.
52. Paxinos G, Franklin KBJ. The Mouse Brain in Stereotaxic Coordinates. 2nd ed. San Diego: Academic Press. 2001.
53. Planel E, Richter KEG, Nolan CE, Finley JE, Liu L, Wen Y, Krishnamurthy P, Herman M, Wang L, Schachter JB, Nelson RB, Lau LF, Duff KE. Anesthesia leads to tau hyperphosphorylation through inhibition of phosphatase activity by hypothermia. J Neurosci. 2007. https://doi.org/10.1523/JNEUROSCI.4854-06.2007.
54. Plouffe V, Mohamed NV, Rivest-McGraw J, Bertrand J, Lauzon M, Leclerc N. Hyperphosphorylation and cleavage at D421 enhance tau secretion. PLoS ONE. 2012. https://doi.org/10.1371/journal.pone.0036873.
55. Pooler AM, Polydoro M, Wegmann S, Nicholls SB, Spires-Jones TL, Hyman BT. Propagation of tau pathology in Alzheimer's disease: identification of novel therapeutic targets. Alzheimers Res Ther. 2013. https://doi.org/10.1186/alzrt214.
56. Rissman RA, Poon WW, Blurton-Jones M, Oddo S, Torp R, Vitek MP, LaFerla FM, Rohn TT, Cotman CW. Caspase-cleavage of tau is an early event in Alzheimer disease tangle pathology. J Clin Investig. 2004. https://doi.org/10.1172/JCI200420640.
57. Sahara N, Murayama M, Higuchi M, Suhara T, Takashima A. Biochemical distribution of tau protein in synaptosomal fraction of transgenic mice expressing human p301l tau. Front Neurol. 2014. https://doi.org/10.3389/fneur.2014.00026.
58. Salta E, De Strooper B. microRNA-132: a key noncoding RNA operating in the cellular phase of Alzheimer's disease. FASEB J. 2017;31(2):424–33. https://doi.org/10.1096/fj.201601308.
59. Salta E, Sierksma A, Vanden Eynden E, De Strooper B. miR-132 loss de-represses ITPKB and aggravates amyloid and TAU pathology in Alzheimer's brain. EMBO Mol Med. 2016;8(9):1005–18. https://doi.org/10.15252/emmm.201606520.
60. Santacruz K, Lewis J, Spires T, Paulson J, Kotilinek L, Ingelsson M, Guimaraes A, DeTure M, Ramsden M, McCowan E, Forster C, Yue M, Orne J, Janus C, Mariash A, Kuskowski M, Hyman B, Hutton M, Ashe KH. Medicine: tau suppression in a neurodegenerative mouse model improves memory function. Science. 2005;309(5733):476–81. https://doi.org/10.1126/science.1113694.
61. Scott L, Kiss T, Kawabe TT, Hajós M. Neuronal network activity in the hippocampus of tau transgenic (Tg4510) mice. Neurobiol Aging. 2016. https://doi.org/10.1016/j.neurobiolaging.2015.10.002.
62. Selenica MLB, Alvarez JA, Nash KR, Lee DC, Cao C, Lin X, Reid P, Mouton PR, Morgan D, Gordon MN. Diverse activation of microglia by chemokine (C-C motif) ligand 2 overexpression in brain. J Neuroinflammation. 2013. https://doi.org/10.1186/1742-2094-10-86.
63. Selenica ML, Benner L, Housley SB, Manchec B, Lee DC, Nash KR, Kalin J, Bergman JA, Kozikowski A, Gordon MN, Morgan D. Histone deacetylase 6 inhibition improves memory and reduces total tau levels in a mouse model of tau deposition. Alzheimers Res Ther. 2014. https://doi.org/10.1186/alzrt241.
64. Shelton LB, Baker JD, Zheng D, Sullivan LE, Solanki PK, Webster JM, Sun Z, Sabbagh JJ, Nordhues BA, Koren J, Ghosh S, Blagg BSJ, Blair LJ, Dickey CA. Hsp90 activator Aha1 drives production of pathological tau aggregates. Proc Natl Acad Sci USA. 2017. https://doi.org/10.1073/pnas.1707039114.
65. Sokolow S, Henkins KM, Bilousova T, Gonzalez B, Vinters HV, Miller CA, Cornwell L, Poon WW, Gylys KH. Pre-synaptic C-terminal truncated tau is released from cortical synapses in Alzheimer's disease. J Neurochem. 2015. https://doi.org/10.1111/jnc.12991.
66. Spillantini MG, Goedert M. Tau pathology and neurodegeneration. Lancet Neurol. 2013. https://doi.org/10.1016/S1474-4422(13)70090-5.
67. Sydow A, Mandelkow EM. "Prion-like" propagation of mouse and human tau aggregates in an inducible mouse model of tauopathy. Neurodegener Dis. 2010. https://doi.org/10.1159/000283479.
68. Taylor R, Neufeld RWJ, Schaefer B, Densmore M, Rajakumar N, Osuch EA, Williamson PC, Théberge J. Functional magnetic resonance spectroscopy of glutamate in schizophrenia and major depressive disorder: anterior cingulate activity during a color-word Stroop task. NPJ Schizophr. 2015;1(1):15028. https://doi.org/10.1038/npjschz.2015.28.

69. Tracy TE, Sohn PD, Minami SS, Wang C, Min SW, Li Y, Zhou Y, Le D, Lo I, Ponnusamy R, Cong X, Schilling B, Ellerby LM, Huganir RL, Gan L. Acetylated tau obstructs KIBRA-mediated signaling in synaptic plasticity and promotes tauopathy-related memory loss. Neuron. 2016;90(2):245–60. https://doi.org/10.1016/j.neuron.2016.03.005.
70. Trotter J, Lee GH, Kazdoba TM, Crowell B, Domogauer J, Mahoney HM, Franco SJ, Müller U, Weeber EJ, D'Arcangelo G. Dab1 is required for synaptic plasticity and associative learning. J Neurosci. 2013. https://doi.org/10.1523/JNEUROSCI.2010-13.2013.
71. Usenovic M, Niroomand S, Drolet RE, Yao L, Gaspar RC, Hatcher NG, Schachter J, Renger JJ, Parmentier-Batteur S. Internalized tau oligomers cause neurodegeneration by inducing accumulation of pathogenic tau in human neurons derived from induced pluripotent stem cells. J Neurosci. 2015;35(42):14234–50. https://doi.org/10.1523/JNEUROSCI.1523-15.2015.
72. Wegmann S, Bennett RE, Delorme L, Robbins AB, Hu M, McKenzie D, Kirk MJ, Schiantarelli J, Tunio N, Amaral AC, Fan Z, Nicholls S, Hudry E, Hyman BT. Experimental evidence for the age dependence of tau protein spread in the brain. Sci Adv. 2019;5(6):6404–30. https://doi.org/10.1126/sciadv.aaw6404.
73. Wieczorek L, Majumdar D, Wills TA, Hu L, Winder DG, Webb DJ, Muglia LJ. Absence of Ca 2+-stimulated adenylyl cyclases leads to reduced synaptic plasticity and impaired experience-dependent fear memory. Transl Psychiatry. 2012;2(5):e126–e126. https://doi.org/10.1038/tp.2012.50.
74. Williams DR. Tauopathies: classification and clinical update on neurodegenerative diseases associated with microtubule-associated protein tau. Intern Med J. 2006. https://doi.org/10.1111/j.1445-5994.2006.01153.x.
75. Woodhall G, Evans DI, Cunningham MO, Jones RSG. NR2B-containing NMDA autoreceptors at synapses on entorhinal cortical neurons. J Neurophysiol. 2001;86(4):1644–51. https://doi.org/10.1152/jn.2001.86.4.1644.
76. Wray S, Saxton M, Anderton BH, Hanger DP. Direct analysis of tau from PSP brain identifies new phosphorylation sites and a major fragment of N-terminally cleaved tau containing four microtubule-binding repeats. J Neurochem. 2008;105(6):2343–52. https://doi.org/10.1111/j.1471-4159.2008.05321.x.
77. Wu JW, Herman M, Liu L, Simoes S, Acker CM, Figueroa H, Steinberg JI, Margittai M, Kayed R, Zurzolo C, Di Paolo G, Duff KE. Small misfolded tau species are internalized via bulk endocytosis and anterogradely and retrogradely transported in neurons. J Biol Chem. 2013. https://doi.org/10.1074/jbc.M112.394528.
78. Xia X, Jiang Q, McDermott J, Han JJ. Aging and Alzheimer's disease: Comparison and associations from molecular to system level. Aging Cell. 2018;17(5):e12802. https://doi.org/10.1111/acel.12802.
79. Yue M, Hanna A, Wilson J, Roder H, Janus C. Sex difference in pathology and memory decline in rTg4510 mouse model of tauopathy. Neurobiol Aging. 2011. https://doi.org/10.1016/j.neurobiolaging.2009.04.006.
80. Zhang Q, Zhang X, Sun A. Truncated tau at D421 is associated with neurodegeneration and tangle formation in the brain of Alzheimer transgenic models. Acta Neuropathol. 2009. https://doi.org/10.1007/s00401-009-0491-6.
81. Zhang Z, Song M, Liu X, Kang SS, Kwon IS, Duong DM, Seyfried NT, Hu WT, Liu Z, Wang JZ, Cheng L, Sun YE, Yu SP, Levey AI, Ye K. Cleavage of tau by asparagine endopeptidase mediates the neurofibrillary pathology in Alzheimer's disease. Nat Med. 2014;20(11):1254–62. https://doi.org/10.1038/nm.3700.
82. Zhao X, Kotilinek LA, Smith B, Hlynialuk C, Zahs K, Ramsden M, Cleary J, Ashe KH. Caspase-2 cleavage of tau reversibly impairs memory. Nat Med. 2016;22(11):1268–76. https://doi.org/10.1038/nm.4199.